Resonance Raman Spectroscopy, and Its Application to Inorganic Chemistry

By Robin J. H. Clark* and Trevor J. Dines

Resonance Raman spectra are obtained when the wave number of the exciting radiation is close to, or coincident with, that of an electronic transition of the scattering species. Such spectra are usually characterized by a very large enhancement of the intensities of particular Raman bands, sometimes with the appearance of intense overtone and combination tone progressions. The technique provides detailed information about excited electronic states because it is only the vibrational modes associated with the chromophore that are resonance-Raman active. Additionally, the high sensitivity is such that compounds at concentrations as low as 10^{-6} mol/L may be detected, enabling resonance Raman spectroscopy to be used as an analytical tool and for the study of chromophores in molecules of biological interest.

1. Introduction

The theory and practice of resonance Raman (RR) spectroscopy have both been developed substantially over the past decade to the extent that it is now possible to present a coherent picture of the subject within the confines of a single article. The object of the present review is to do this in a readily comprehendable manner and also to review the applications of the subject within the broad bounds of inorganic chemistry. To this end, Section 2 relates to the theoretical development of the subject, as it now stands. In particular, the relation between normal and RR scattering is developed, as is the nature of A-, B-, C- and D-term scattering, and scattering by both totally symmetric and non-totally symmetric modes. The significance of the depolarization ratio of a Raman band is also outlined, both with respect to vibrational as well as electronic band assignments.

Following a discussion of experimental techniques in Section 3, the results of many studies of inorganic compounds are then reviewed beginning with diatomic species and progressing through increasingly complicated species to metalloporphyrins and related species. In order to achieve conciseness this section has been restricted to RR studies reported since 1977, a comprehensive compilation of the earlier work being available already.[1] The investigations of small molecules (Section 4) have been considered in detail because these have contributed most to the understanding of the RR effect. The discussion of larger molecules (Section 5) has been restricted to a few illustrative examples and the reader is referred to reviews dealing specifically with metal-metal bonded species,[2] mixed-valence molecules,[3,4] and metalloporphyrins.[5] The attention of the reader is also directed elsewhere for reviews of RR studies on semiconductors,[6] electronic Raman scattering,[7] and time-resolved resonance Raman (TR³) experiments.[8]

Many people have contributed to the development of experimental and theoretical aspects of the subject, notably Albrecht,[9-12] Shorygin,[13,14] Behringer,[15,16] Peticolas,[17,18] Koningstein,[19-21] Rousseau et al.,[22] Clark,[1,23,24] Stewart,[1,24] Spiro,[25-27] Kiefer,[28] Tsuboi,[29,30] Mortensen,[31] Siebrand and Zgierski,[32] Barron,[33,34] Hong,[35] and Heller.[36,37] Although a variety of different systems of nomenclature have been used to present the subject, that adopted in this review is essentially due to Clark and Dines.[7,38]

The central feature of interest in RR spectroscopy is the fact that, when the wave number of the exciting line is made to coincide with that of an allowed electronic transition in a molecule, the intensities of certain Raman bands of the scattering molecule are greatly enhanced relative to their off-resonance values. Thus the technique is a much more sensitive one than is normal Raman spectroscopy. Moreover, it proves to be a much more specific technique in the sense that it is solely modes to do with the chromophore in the scattering molecule which can be enhanced at resonance. Thus, information relating to the chemically significant parts of molecules is obtainable by this form of Raman spectroscopy. RR spectroscopy can also be applied to the determination of the displacements of the potential surfaces of excited states relative to that of the ground state, a matter of considerable importance in spectroscopy, photophysics, and photochemistry. The manner in which this may be done is outlined in the following pages.

2. Theory of Resonance Raman Scattering

In this section the theoretical approach that is most commonly used in the interpretation of RR data is outlined, based on the earlier developments of Albrecht et al.[9,10] and Shorygin et al.[13,14] RR scattering is described, in the energy-frame, in terms of the Kramers-Heisenberg dispersion formula,[39] obtained by second-order perturbation theory. Other approaches that have been described recently include the time correlator theory[36,37] and the optical transform theory.[11,12] These are claimed to be able to

[*] Prof. Dr. R. J. H. Clark and Dr. T. J. Dines
Christopher Ingold Laboratories
University College London
20 Gordon Street, London WC1H 0AJ (UK)

deal more easily with polyatomic molecules in which several modes are RR-active, but this view is not yet generally accepted.

For a Raman transition between two states $|i\rangle$ and $|f\rangle$ of a scattering system, the intensity of light scattered at $90°$ to the direction of irradiation is given by Equation (1).

$$I_{fi}(\pi/2) = \frac{\pi^2}{\varepsilon_0^2}(\bar{\nu}_0 \pm \bar{\nu}_{fi})^4 \mathscr{I}_0 \sum_{\rho,\sigma}[\alpha_{\rho\sigma}]_{fi}[\alpha_{\rho\sigma}]_{fi}^* \tag{1}$$

$\mathscr{I}_0$ is the irradiance of the incident radiation, $\bar{\nu}_0$ and $\bar{\nu}_{fi}$ are the wave numbers of the exciting line and of the Raman transition $|f\rangle \leftarrow |i\rangle$, respectively, ε_0 is the permittivity of free space, and $[\alpha_{\rho\sigma}]_{fi}$ is the $\rho\sigma$th element of the transition polarizability tensor [Eqn. (2)].

$$[\alpha_{\rho\sigma}]_{fi} = \frac{1}{hc}\sum_r\left[\frac{[\mu_\rho]_{fr}[\mu_\sigma]_{ri}}{\bar{\nu}_{ri}-\bar{\nu}_0+i\Gamma_r} + \frac{[\mu_\sigma]_{fr}[\mu_\rho]_{ri}}{\bar{\nu}_{rf}+\bar{\nu}_0+i\Gamma_r}\right] \tag{2}$$

In this equation $[\mu_\rho]_{fr}$ is the ρth component of the transition dipole moment associated with the transition $|f\rangle \leftarrow |r\rangle$ and $i\Gamma_r$ is a damping factor, which is related to the lifetime of the state $|r\rangle$. Strictly, the summation is over all states $|r\rangle$ of the system, including $|i\rangle$ and $|f\rangle$, but it has been shown that, for Raman scattering, $|i\rangle$ and $|f\rangle$ may be excluded from the sum.[40] (In the SI system, I is in W, $\mathscr{I}_0$ in W m^{-2}, ε_0 in F m^{-1}, $[\alpha_{\rho\sigma}]_{fi}$ in C V^{-1} m^2 and $[\mu_\rho]_{fr}$ in C m. The use of the unit cm^{-1} for wave number requires that the right-hand side of Equation (2) be multiplied by 10^8.) For vibrational Raman scattering excited far from resonance, the tensor is symmetric, i.e. $\alpha_{\rho\sigma}=\alpha_{\sigma\rho}$, but it may become asymmetric for electronic Raman (ER) and RR scattering.

The nature of the Raman effect is determined by the initial and final eigenstates $|i\rangle$ and $|f\rangle$, and by the proximity of the wave number of the exciting radiation to that of any electronic transition of the system. Clearly, the RR effect occurs when $\bar{\nu}_0 \approx \bar{\nu}_{ri}$, resulting in an increase of $[\alpha_{\rho\sigma}]_{fi}$ and consequently an enhancement of the Raman intensity. In order to answer such questions as which Raman bands may undergo enhancement and why overtone progressions are observed in RR spectra it is necessary to probe the dependence of $[\alpha_{\rho\sigma}]_{fi}$ on the properties of excited states by looking closely at Equation (2). As a prelude to such an analysis it is instructive to consider first the case of normal, i.e. non-RR scattering.

2.1. Normal Raman Scattering

The adiabatic Born-Oppenheimer approximation is invoked, in which the vibronic states $|i\rangle$, $|f\rangle$, and $|r\rangle$ are formed by products of the pure vibrational and the pure electronic states. The latter are referred to some fixed positions of the nuclei and are parametrically dependent on the normal coordinates, Q_k, of the molecule.

Assuming that the system is initially and finally in the ground electronic state $|g\rangle$ (i.e. a vibrational Raman transition, for instance, is under consideration), we may write:

$$\begin{aligned}|i\rangle &= |gm\rangle = |g\rangle|m\rangle\\ |f\rangle &= |gn\rangle = |g\rangle|n\rangle\\ |r\rangle &= |ev\rangle = |e\rangle|v\rangle\end{aligned} \tag{3}$$

where $|e\rangle$ represents an excited electronic state and $|m\rangle$, $|n\rangle$, and $|v\rangle$ represent vibrational states of the scattering species. This enables the transition polarizability to be rewritten in the form

$$[\alpha_{\rho\sigma}]_{gn,gm} = \frac{1}{hc}\sum_{ev}\left(\frac{\langle n|[\mu_\rho]_{ge}|v\rangle\langle v|[\mu_\sigma]_{eg}|m\rangle}{\bar{\nu}_{ev,gm}-\bar{\nu}_0+i\Gamma_{ev}}\right.$$
$$\left. + \frac{\langle n|[\mu_\sigma]_{ge}|v\rangle\langle v|[\mu_\rho]_{eg}|m\rangle}{\bar{\nu}_{ev,gn}+\bar{\nu}_0+i\Gamma_{ev}}\right) \tag{4}$$

where $[\mu_\rho]_{ge}$ is the pure electronic transition moment associated with the transition $|g\rangle\leftarrow|e\rangle$. Under the conditions for which the Born-Oppenheimer condition is valid, the dependence of such an electronic transition moment on the k normal coordinates of the system, Q_k, is small. Thus, $[\mu_\rho]_{ge}$ may be expressed as a rapidly converging Taylor series expanded around the equilibrium position:

$$[\mu_\rho]_{ge} = [\mu_\rho]_{ge}^0 + \sum_k[\mu_\rho]_{ge}'Q_k + \cdots \tag{5}$$

where $[\mu_\rho]_{ge}' = \partial[\mu_\rho]_{ge}/\partial Q_k$. Higher order terms in this series are, in most cases, negligibly small. A second simplification arises from the Born-Oppenheimer approximation in that the electronic and vibrational parts of the integrals in Equation (4) may be separated, such that, for example

$$\langle n|[\mu_\rho]_{ge}|v\rangle = [\mu_\rho]_{ge}^0\langle n|v\rangle + \sum_k[\mu_\rho]_{ge}'\langle n|Q_k|v\rangle \tag{6}$$

The following approximations may also be made in the ideal limit of excitation far from any region of electronic absorption:

(1) The denominators in the transition polarizability are large and insensitive to the vibrational quantum numbers m, n, and v, such that differences between the various $\bar{\nu}_{ev,gm}$ and $\bar{\nu}_{ev,gn}$ may be neglected;

(2) The states $|v\rangle$ represent a complete orthonormal set and the sums over them may be evaluated by invoking the closure theorem, which states that $\sum_v|v\rangle\langle v| = 1$, and arises from the matrix product rule $\sum_j A_{ij}B_{jk} = (AB)_{ik}$;

(3) Since $(\bar{\nu}_{ev,gm}-\bar{\nu}_0)$ and $(\bar{\nu}_{eg,gn}+\bar{\nu}_0)$ are much larger than the damping factors, $i\Gamma_{ev}$, the latter may be neglected.

With these approximations, and noting that

$$(\bar{\nu}_e-\bar{\nu}_0)^{-1} + (\bar{\nu}_e+\bar{\nu}_0)^{-1} = 2\bar{\nu}_e(\bar{\nu}_e^2-\bar{\nu}_0^2)^{-1}$$

the transition polarizability may be recast in the following form:

$$\begin{aligned}[\alpha_{\rho\sigma}]_{gn,gm} &= \frac{1}{hc}\sum_e\frac{2\bar{\nu}_e}{(\bar{\nu}_e^2-\bar{\nu}_0^2)}[\mu_\rho]_{ge}^0[\mu_\sigma]_{eg}^0\langle n|m\rangle\\ &+ \frac{1}{hc}\sum_e\sum_k\frac{2\bar{\nu}_e}{(\bar{\nu}_e^2-\bar{\nu}_0^2)}\{[\mu_\rho]_{ge}'[\mu_\sigma]_{eg}^0 + [\mu_\rho]_{ge}^0[\mu_\sigma]_{eg}'\}\langle n|Q_k|m\rangle\\ &+ \frac{1}{hc}\sum_e\sum_{k,k'}\frac{2\bar{\nu}_e}{(\bar{\nu}_e^2-\bar{\nu}_0^2)}[\mu_\rho]_{ge}'[\mu_\sigma]_{eg}'\langle n|Q_kQ_{k'}|m\rangle\end{aligned} \tag{7}$$

Because n and m are both vibrational quantum numbers of the ground electronic state, the overlap integral

132

Angew. Chem. Int. Ed. Engl. 25 (1986) 131-158

$\langle n|m \rangle = \delta_{nm}$. Thus, the first term in Equation (7) contributes only to Rayleigh scattering. The integral $\langle n|Q_k|m \rangle$ is non-zero if $n = m \pm 1$ and has the value $[h(m+1)/8\pi^2 c \bar{v}_k]^{1/2}$ for $n = m + 1$ and $[hm/8\pi^2 c \bar{v}_k]^{1/2}$ for $n = m - 1$. It follows that the second term in Equation (7) is responsible for both the Stokes and the anti-Stokes Raman scattering for vibrational fundamentals. The third term gives rise to first overtones ($k = k'$) and binary combination tones ($k \neq k'$), but is usually so small that bands so attributed are very weak in normal Raman scattering. It is obvious that the magnitude of $[\alpha_{\rho\sigma}]_{gn,gm}$ is unaffected by transposition of the coordinate suffixes ρ and σ. Hence the transition polarizability tensor is symmetric about the leading diagonal and has only six independent components. It may be regarded essentially as a ground state property of the system.

2.2. Resonance Raman Scattering

In the usual treatment of RR scattering the adiabatic Born-Oppenheimer approximation is assumed to be valid, but the other assumptions associated with normal Raman scattering are assumed no longer to apply. That is to say:

(1) The v-dependence of the denominators in Equation (4) cannot be neglected, so that the closure theorem may not be invoked;

(2) the wave-number difference ($\bar{v}_{ev,gm} - \bar{v}_0$) is comparable with the damping factor, $i\Gamma_{ev}$, so that the latter may not be neglected;

(3) the first-order term $\partial[\mu_\rho]_{ge}/\partial Q_k = [\mu_\rho]'_{ge}$ in the Taylor expansion of Equation (5) needs to be defined explicitly.

In the Herzberg-Teller[41] perturbation description of vibronic coupling the derivative of the transition moment arises because the variation in the Hamiltonian with respect to the normal coordinate Q_k can mix the state $|e\rangle$ with other states $|s\rangle$ of the appropriate symmetry, viz.

$$[\mu_\rho]_{ge} = [\mu_\rho]^0_{ge} + \sum_s \sum_k [\mu_\rho]^0_{gs} \frac{h^k_{es}}{\Delta \bar{v}_{es}} Q_k + \cdots \qquad (8)$$

$$h^k_{es} = \langle e|\partial H/\partial Q_k|s\rangle_{Q_{k=0}}$$

where $|s\rangle$ represents another excited state. As before, higher order terms are generally negligible.

The term $h^k_{es}/\Delta \bar{v}_{es}$ is a measure of the strength of vibronic coupling of the states $|e\rangle$ and $|s\rangle$ via the normal coordinate Q_k. The Herzberg-Teller expansion is only valid for weak vibronic coupling, i.e. within the framework of the adiabatic Born-Oppenheimer approximation. It is not applicable to cases in which there is strong vibronic coupling, i.e. when $\Delta \bar{v}_{es}$ is of the order of vibrational wave numbers (in which case non-adiabatic coupling is important) or zero (such as for a degenerate state, in which Jahn-Teller (JT) coupling occurs).

Some considerable simplification of the transition polarizability is made possible for excitation under resonance conditions. This is because, as $\bar{v}_0$ approaches some particular transition wave number $\bar{v}_{ev,gm}$, the relevant excited state will dominate the sum over states. It is therefore generally

sufficient to consider only one, or at most, two electronic manifolds. Also, the non-resonant part of the transition polarizability may be neglected at resonance. Applying these considerations to Equation (4) it is evident that there are now four contributions (the so-called A, B, C, and D-terms) to the transition polarizability, viz.

$$[\alpha_{\rho\sigma}]_{gn,gm} = A + B + C + D \qquad (9)$$

where

$$A = \frac{1}{hc} [\mu_\rho]^0_{ge} [\mu_\sigma]^0_{eg} \sum_v \frac{\langle n_g|v_e\rangle \langle v_e|m_g\rangle}{\bar{v}_{ev,gm} - \bar{v}_0 + i\Gamma_{ev}} \qquad (10)$$

$$B = \frac{1}{h^2 c^2} \sum_{s \neq e} [\mu_\rho]^0_{gs} [\mu_\sigma]^0_{eg} \frac{h^k_{se}}{\Delta \bar{v}_{se}} \sum_v \frac{\langle n_g|Q_k|v_e\rangle \langle v_e|m_g\rangle}{\bar{v}_{ev,gm} - \bar{v}_0 + i\Gamma_{ev}}$$
$$+ \frac{1}{h^2 c^2} \sum_{s \neq e} [\mu_\rho]^0_{ge} [\mu_\sigma]^0_{sg} \frac{h^k_{es}}{\Delta \bar{v}_{es}} \sum_v \frac{\langle n_g|v_e\rangle \langle v_e|Q_k|m_g\rangle}{\bar{v}_{eg,gm} - \bar{v}_0 + i\Gamma_{ev}} \qquad (11)$$

$$C = \frac{1}{h^2 c^2} \sum_{s \neq g} [\mu_\rho]^0_{se} [\mu_\sigma]^0_{eg} \frac{h^k_{gs}}{\Delta \bar{v}_{gs}} \sum_v \frac{\langle n_g|Q_k|v_e\rangle \langle v_e|m_g\rangle}{\bar{v}_{ev,gm} - \bar{v}_0 + i\Gamma_{ev}}$$
$$+ \frac{1}{h^2 c^2} \sum_{s \neq g} [\mu_\rho]^0_{ge} [\mu_\sigma]^0_{es} \frac{h^k_{sg}}{\Delta \bar{v}_{sg}} \sum_v \frac{\langle n_g|v_e\rangle \langle v_e|Q_k|m_g\rangle}{\bar{v}_{ev,gm} - \bar{v}_0 + i\Gamma_{ev}} \qquad (12)$$

$$D = \frac{1}{h^3 c^3} \sum_{s,s' \neq e} [\mu_\rho]^0_{gs} [\mu_\sigma]^0_{s'g} \frac{h^k_{es} h^{k'}_{es'}}{\Delta \bar{v}_{es} \Delta \bar{v}_{es'}} \sum_v \frac{\langle n_g|Q_k|v_e\rangle \langle v_e|Q_{k'}|m_g\rangle}{\bar{v}_{ev,gm} - \bar{v}_0 + i\Gamma_{ev}} \qquad (13)$$

In these equations the vibrational quantum numbers n, v and m have been subscripted to indicate the electronic state to which they refer, all other terms having been defined previously. We now look closely at each of these four contributions.

2.2.1. A-term Resonance Raman Scattering

For the A-term contribution to the transition polarizability to be non-zero it is necessary that the following two conditions are fulfilled:

(1) The transition dipole moments $[\mu_\rho]^0_{ge}$ and $[\mu_\sigma]^0_{eg}$ must be non-zero;

(2) The products of vibrational overlap integrals (Franck-Condon factors), $\langle n_g|v_e\rangle \langle v_e|m_g\rangle$, must be non-zero for at least some values of v.

The first of these two conditions dictates that the resonant electronic transition should be electric-dipole-allowed. Thus the technique requires excitation within the contour of an intense absorption band, such as one of charge transfer (CT) or π-π^* type. Excitation within the contour of a weak band, e.g. one resulting from a ligand-field or spin-forbidden transition, would not be expected to produce a significant A-term. The restrictions imposed by the second condition are less obvious and therefore warrant a more detailed discussion.

Vibrational overlap integrals of the type $\langle n_g|v_e\rangle$ are zero (except for the case $n = v$) unless the vibrational wave functions χ_n and χ_v are non-orthogonal. For any one vibrational mode v_k of a molecule non-orthogonality of these wave functions will subsist if, between the ground state and excited states, there is either (a) a difference of vibrational wave number ($\bar{v}^e_k \neq \bar{v}^g_k$), i.e. a change in shape of the

Angew. Chem. Int. Ed. Engl. 25 (1986) 131-158

133

potential energy surface, or (b) a displacement of the potential energy minimum along the normal coordinate, ΔQ_k. Symmetry arguments dictate that such a displacement may only occur for totally symmetric modes unless the molecular symmetry is altered in the excited state. If the molecular symmetry is the same in the ground and excited states, then geometric changes are confined to combinations of alterations in bond lengths and bond angles that, overall, do not change the molecular symmetry. Thus, the geometric changes are confined to those along totally symmetric symmetry coordinates which, of course, relate only to displacements along totally symmetric normal coordinates. However, if a change of molecular symmetry accompanies the electronic transition, this restriction no longer applies. The term totally symmetric then applies not to the ground state point group but to the subgroup formed by the operations that are common to both the ground- and excited-state point groups (the common group).

As shown in Figure 1, four cases (a)—(d) may be distinguished: It is obvious that in case (a) the orthogonality of the wave functions would not be removed and in such a situation there would be no A-term for any vibrational mode. Case (b) produces non-zero overlap integrals for both totally and non-totally symmetric modes, whereas cases (c) and (d) only apply to totally symmetric modes. In practice it is found that a significant change of vibrational wave number usually occurs only where there is a displacement of the potential energy minimum, hence case (d) is the most important. Dependent on the magnitude of ΔQ, the Franck-Condon factors, $\langle n_g|v_e\rangle\langle v_e|m_g\rangle$, may have appreciable size for up to several quanta of n. Thus the A-term can give rise to overtones of intensity comparable to that of the fundamental.
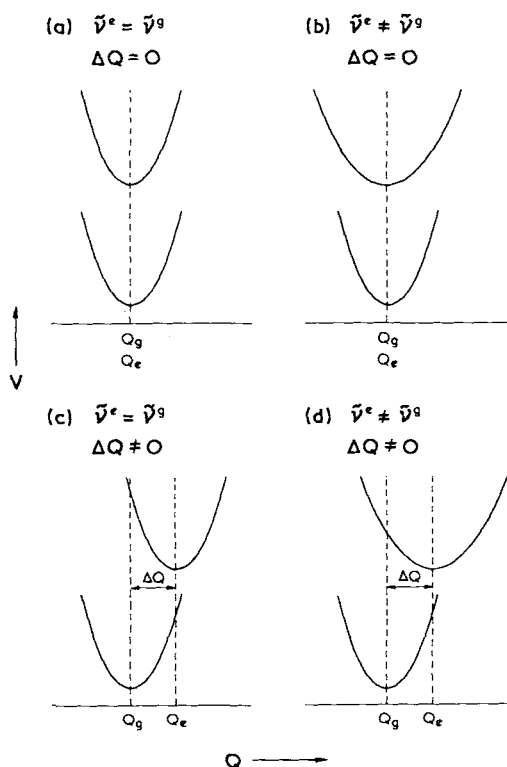
2.2.2. B-Term Resonance Raman Scattering

The B-term contribution to the transition polarizability arises from the vibronic coupling of the resonant state to other excited states. Its magnitude is dependent on the vibronic coupling integral h_{es}^k, on the products of vibrational transition integrals and overlap integrals, e.g. $\langle n_g|Q_k|v_e\rangle\langle v_e|m_g\rangle$, on the transition dipole moments $[\mu_\rho]_{ge}^0$ and $[\mu_\sigma]_{sg}^0$, and on the energy difference between the coupled states, $hc(\bar{v}_s - \bar{v}_e)$. For the B-term to be non-zero it is a requirement that both the resonant transition and the transition $|s\rangle \leftarrow |g\rangle$ should be electric-dipole-allowed. Because of the additional factor $h_{es}^k(v_s - v_e)^{-1}$in the equation, the B-term is usually very much smaller than the A-term. However, if the resonant transition gives rise to zero or very small displacements ΔQ_k, then only the diagonal overlap integrals (i.e. n = v, v = m) are non-vanishing and the A-term becomes zero. In the harmonic oscillator approximation $\langle n_g|Q_k|v_e\rangle$ and $\langle v_e|Q_k|m_g\rangle$ are non-zero for $n = v \pm 1$ and $v = m \pm 1$. Thus, under the conditions for which the B-term is of importance (diagonal overlap integrals) the products $\langle n_g|Q_k|v_e\rangle\langle v_e|m_g\rangle$ and $\langle n_g|v_e\rangle\langle v_e|Q_k|m_g\rangle$ are restricted to the cases where $n = m \pm 1$ and, in the low temperature limit (m = 0), only two such products would contribute, viz. $\langle 1_g|Q_k|0_e\rangle\langle 0_e|0_g\rangle$ and $\langle 1_g|1_e\rangle\langle 1_e|Q_k|0_g\rangle$. It is usually the case that coupling to only one other state $|s\rangle$ needs to be considered and the summation may be dropped, giving the following expression for the B-term:

$$B = \frac{1}{h^2c^2}[\mu_\rho]_{gs}^0 [\mu_\sigma]_{eg}^0 \frac{h_{se}^k}{\Delta\bar{v}_{se}}\left(\frac{\langle 1_g|Q_k|0_e\rangle\langle 0_e|0_g\rangle}{\bar{v}_{e0,g0} - \bar{v}_0 + i\Gamma_{e0}}\right)$$
$$+ \frac{1}{h^2c^2}[\mu_\rho]_{ge}^0 [\mu_\sigma]_{sg}^0 \frac{h_{es}^k}{\Delta\bar{v}_{es}}\left(\frac{\langle 1_g|1_e\rangle\langle 1_e|Q_k|0_g\rangle}{\bar{v}_{e1,g0} - \bar{v}_0 + i\Gamma_{e1}}\right) \tag{14}$$

Clearly, B-term scattering occurs only for fundamentals (n = 1) and the symmetry selection rules are constrained by the symmetries of the states $|e\rangle$ and $|s\rangle$. The vibronic coupling integral h_{es}^k is non-zero if the irreducible representation of Q_k (i.e. Γ_k) is contained in the direct product $\Gamma_e \otimes \Gamma_s$. It follows that B-term activity may be expected for both totally symmetric and non-totally symmetric vibrations, but for the former to be realized it is necessary that $|e\rangle$ and $|s\rangle$ have the same symmetry.

2.2.3. C- and D-Term Resonance Raman Scattering

The C-term differs from the B-term in that the ground state, rather than the resonant excited state, is vibronically coupled to other excited states. It is normally assumed that the C-term is negligibly small, due to the large energy separation between the ground state and excited states. To our knowledge no experimental evidence for C-term scattering has yet been presented.

The D-term is also very much smaller than the B-term. It may give rise to first overtones (k = k') and binary combination tones (k ≠ k') of both totally symmetric and non-totally symmetric modes. The observation of weak overtones and binary combination tones in the RR spectra of some metalloporphyrin species has been ascribed to D-term scattering (see Sections 2.4 and 5.4).

Fig. 1. Potential energy diagrams for the ground and resonant excited states, showing the four cases (a)—(d) (see text).

2.3. Resonance Raman Scattering Involving Totally Symmetric Modes

Raman bands attributed to totally symmetric fundamentals may acquire intensity under resonance conditions from either the A- or B-terms of the transition polarizability. It is generally the case, however, that only the A-term contribution is important, for the reasons mentioned in Section 2.2. In this section we discuss in detail the properties of A- and B-term RR scattering for totally symmetric fundamentals and their overtones. To begin with we consider the simplest case of a species possessing only one totally symmetric mode (such as diatomic, tetrahedral or square planar (MX$_4$), or octahedral (MX$_6$) molecules), in which case only diagonal components of the transition polarizability, $[\alpha_{\rho\rho}]_{gn,gm}$, are non-zero. If it is further assumed that (a) only a single resonant excited state $|e\rangle$ makes a significant contribution, and (b) all molecules are initially in the $m = 0$ vibrational level of the ground electronic state (low temperature limit) then

$$[\alpha_{\rho\rho}]_{gn,g0} = \frac{1}{hc} \, |[\mu_\rho]_{ge}^0|^2 \sum_v \frac{\langle n_g|v_e\rangle\langle v_e|0_g\rangle}{\bar{v}_{ev,g0} - \bar{v}_0 + i\Gamma_{ev}} \tag{15}$$

For a system with only one totally symmetric normal coordinate, Q_1, the vibrational overlap integrals are one-dimensional. Assuming harmonic potentials for the states $|g\rangle$ and $|e\rangle$, the overlap integrals may be calculated using the recurrence formulas derived by *Manneback*:[42]

$$\langle 0_e|0_g\rangle = \left(\frac{2(\bar{v}_1^e \bar{v}_1^g)^{1/2}}{\bar{v}_1^e + \bar{v}_1^g}\right)^{1/2} \exp\left(\frac{-\Delta^2}{2}\right) \tag{16a}$$

$$\langle n_g|v_e + 1\rangle = -\left(\frac{v}{v+1}\right)^{1/2}\left(\frac{\bar{v}_1^g - \bar{v}_1^e}{\bar{v}_1^g + \bar{v}_1^e}\right)\langle n_g|v_e - 1\rangle$$
$$+\left(\frac{n}{v+1}\right)^{1/2}\frac{2(\bar{v}_1^e \bar{v}_1^g)^{1/2}}{\bar{v}_1^e + \bar{v}_1^g}\langle n_g - 1|v_e\rangle \tag{16b}$$
$$-\left(\frac{1}{v+1}\right)^{1/2}\Delta\left(\frac{2\bar{v}_1^g}{\bar{v}_1^g + \bar{v}_1^e}\right)^{1/2}\langle n_g|v_e\rangle$$

$$\langle n_g + 1|v_e\rangle = \left(\frac{n}{n+1}\right)^{1/2}\left(\frac{\bar{v}_1^g - \bar{v}_1^e}{\bar{v}_1^g + \bar{v}_1^e}\right)\langle n_g - 1|v_e\rangle$$
$$+\left(\frac{v}{n+1}\right)^{1/2}\frac{2(\bar{v}_1^e \bar{v}_1^g)^{1/2}}{\bar{v}_1^e + \bar{v}_1^g}\langle n_g|v_e - 1\rangle \tag{16c}$$
$$+\left(\frac{1}{n+1}\right)^{1/2}\Delta\left(\frac{2\bar{v}_1^g}{\bar{v}_1^g + \bar{v}_1^e}\right)^{1/2}\langle n_g|v_e\rangle$$

where the dimensionless shift parameter Δ is given by

$$\Delta = \left(\frac{4\pi^2 c}{h}\right)^{1/2}\Delta Q_1\left(\frac{\bar{v}_1^e \bar{v}_1^g}{\bar{v}_1^e + \bar{v}_1^g}\right)^{1/2} \tag{16d}$$

The displacement, ΔQ_1, of the excited-state potential minimum is related to the displacement along the symmetry coordinate ΔS_1 by the equation

$$\Delta Q_1 = \mu^{1/2}\Delta S_1 \tag{17}$$

where μ is the reduced mass associated with the vibration. Expressions for ΔQ_1 in terms of Δr for a number of common molecular geometries are summarized in Table 1.

Table 1. Relationship between ΔQ_1 and Δr for various molecular geometries.

$\Delta Q_1 = \mu^{1/2}\Delta S_1$

Molecular type	Point group	μ	ΔS_1	ΔQ_1
XY	$C_{\infty v}$	$\dfrac{m_x m_y}{m_x + m_y}$	Δr	$\left[\dfrac{m_x m_y}{m_x + m_y}\right]^{1/2}\Delta r$
X$_2$	$D_{\infty h}$	$m_x/2$	Δr	$(m_x/2)^{1/2}\Delta r$
MX$_2$ X$_3$	$D_{\infty h}$	m_x	$\dfrac{1}{\sqrt{2}}(\Delta r_1 + \Delta r_2)$	$(2m_x)^{1/2}\Delta r$
MX$_3$ X$_3$ X$_4$	D_{3h}	m_x	$\dfrac{1}{\sqrt{3}}(\Delta r_1 + \Delta r_2 + \Delta r_3)$	$(3m_x)^{1/2}\Delta r$
MX$_4$ X$_4$	D_{4h}, T_d	m_x	$\dfrac{1}{2}(\Delta r_1 + \Delta r_2 + \Delta r_3 + \Delta r_4)$	$2(m_x)^{1/2}\Delta r$
MX$_6$ X$_6$	O_h	m_x	$\dfrac{1}{\sqrt{6}}(\Delta r_1 + \Delta r_2 + \Delta r_3 + \Delta r_4 + \Delta r_5 + \Delta r_6)$	$(6m_x)^{1/2}\Delta r$

The Franck-Condon overlap integrals may possess appreciable magnitudes for up to several quanta of n if ΔQ_1 is sufficiently large, in which case several overtones of v_1 may appear in the RR spectrum. The intensity distribution within such an overtone progression depends on the magnitude of ΔQ (and hence on the bond length change Δr) and, in general, the larger the displacement the greater is the extent of the progression. Thus, excitation resonant with charge-transfer or π-π^* transitions of small molecules typically produces RR spectra that are characterized by an intense overtone progression $v_1 v_1$.

Substitution of Equation (15) into Equation (1) and expansion of the square modulus of $[\alpha_{\rho\rho}]_{gn,g0}$ gives the following expression for Stokes A-term RR intensities:

$$I_{gn,g0}(\pi/2) = K(\bar{v}_0 - \bar{v}_{gn,g0})^4 \, |[\mu_\rho]_{ge}^0|^4$$
$$\times \sum_v \sum_{v'} \frac{\langle n_g|v_e\rangle\langle v_e|0_g\rangle\langle n_g|v_e'\rangle\langle v_e'|0_g\rangle[\varepsilon_v \varepsilon_{v'} + \Gamma_v \Gamma_{v'}]}{(\varepsilon_v^2 + \Gamma_v^2)(\varepsilon_{v'}^2 + \Gamma_{v'}^2)} \tag{18}$$

where $\varepsilon_v = \bar{v}_{ev,g0} - \bar{v}_0$ and K incorporates all of the constants appearing in Equations (1) and (15). From this expression it is possible to calculate the variation of the intensities of the fundamental and overtone bands throughout the region of the resonant absorption band. Such a plot, which is called an excitation profile (EP), differs markedly from the absorption spectrum if the vibrational fine structure of the latter is resolved (small Γ). Whereas absorption profiles are simply given by the superposition (i.e. sum) of the individual vibronic bands, the double summation in Equation (18) involves cross-terms ($v \neq v'$) which produce interference between the contributions from different vibronic states. These interference effects may result in an increase or decrease in scattered intensity compared with that arising solely from the sum of the individual resonances ($v = v'$). However, when Γ is large these interferences are not apparent and both the excitation profiles and the absorption spectrum are smooth and devoid of fine structure. The maxima of the excitation profiles are then blue-shifted for successive overtones, the differ-
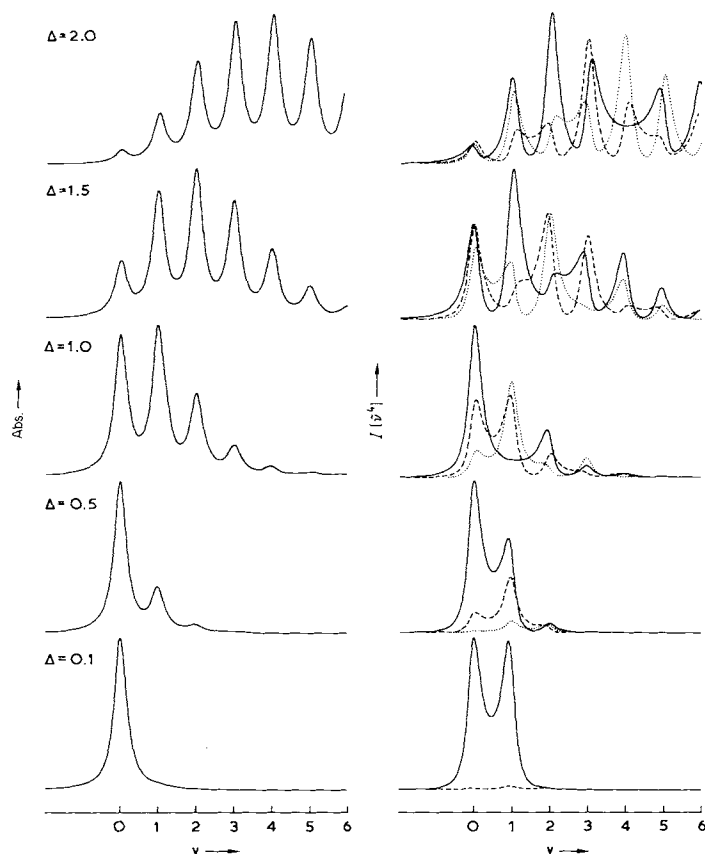
Fig. 2. Left, Absorption spectra, and right, resonance Raman excitation profiles (v_1 (——), $2 v_1$ (---) and $3 v_1$ (····) bands) for different values of the shift parameter Δ; $\bar{v}^e = \bar{v}^g$ and $\Gamma = 0.2 \bar{v}^e$ (abscissa is expressed in terms of excited-state vibrational quanta v). Abs = Absorption, I = Raman intensity.

ence in peak position being approximately equal to the vibrational wave number of the excited state.

In Figure 2 is shown the effect of the displacement parameter Δ on Raman intensities. For simplicity a model system has been chosen in which $\bar{v}^e = \bar{v}^g$ and $\Gamma = 0.2 \bar{v}^e$ and the EPs are displayed for v_1, $2 v_1$ and $3 v_1$ for several values of Δ. These profiles clearly demonstrate the above-mentioned interference effects and it is evident that EPs are more sensitive to variation in Δ than are absorption bands. It is readily seen that, as Δ increases, the EP maximum is shifted to higher wave number and that the intensities of overtones increase with respect to that of the fundamental, becoming the more intense in some regions.

By fitting calculated excitation profiles to experimental data the parameters Δ and Γ may be extracted. Thus, the technique provides a sensitive method for the determination of excited state geometries and lifetimes and several results of such calculations are discussed in later sections. It is, however, important to appreciate that lifetime, i.e. homogeneous, broadening is not the only contribution to bandwidths and that the influence of inhomogeneous broadening must also be taken into account. Inhomogeneous broadening is due to the variation of molecular environment (i.e. molecules occupying different sites) and the "spread" of electronic energies resulting from it is described by a Gaussian or Lorentzian distribution about the mean value. Although a Gaussian distribution would normally be the correct description of inhomogeneous broadening, the influence of the band shape is not very great and

a Lorentzian function is usually chosen for simplicity.[43,44] The inhomogeneous band shape is then given by

$$\mathscr{S}(\bar{v}) = \frac{\gamma}{[\langle \bar{v}_{e0} \rangle - \bar{v}_{e0}]^2 + \gamma^2} \tag{19}$$

where γ is the inhomogeneous bandwidth (half width at half maximum) and $\langle \bar{v}_{e0} \rangle$ is the average value of the electronic transition wave number. The effect of inhomogeneous broadening on the transition polarizability is taken into account by convolution with the above band-shape function, integrating over all possible values of $\bar{v}_{e0}$:

$$[\alpha_{\rho\rho}]_{gn,g0} = \frac{1}{hc} |[\mu_\rho]_{ge}^0|^2 \int_{-\infty}^{\infty} \left(\sum_v \frac{\langle n_g|v_e\rangle\langle v_e|0_g\rangle}{\bar{v}_{ev,g0} - \bar{v}_0 + i\Gamma_{ev}} \right) \mathscr{S}(\bar{v}) \cdot d\bar{v}_{e0} \tag{20}$$

Such integrals have been evaluated by Siebrand et al.,[43,44] and the following expression is obtained for the Raman intensity:

$$I_{gn,g0}(\pi/2) = K(\bar{v}_0 - \bar{v}_{gn,g0})^4 |[\mu_\rho]_{ge}^0|^4 \sum_v \sum_{v'} \langle n_g|v_e\rangle\langle v_e|0_g\rangle\langle n_g|v_e'\rangle\langle v_e'|0_g\rangle$$

$$\times \left(\frac{[(\varepsilon_v - \varepsilon_{v'})^2 + 4\Gamma\Sigma][\varepsilon_v\varepsilon_{v'} + \Sigma^2] - 2(\varepsilon_v - \varepsilon_{v'})\gamma\Sigma}{[\varepsilon_v^2 + \Sigma^2][\varepsilon_{v'}^2 + \Sigma^2][(\varepsilon_v - \varepsilon_{v'})^2 + 4\Gamma^2]} \right) \tag{21}$$

where $\Sigma = \Gamma + \gamma$.

In most cases Γ is small, rarely exceeding about $0.5 \bar{v}_1^e$, but γ may range from zero (putting $\gamma = 0$ in Equation (21) yields Equation (18)) to a few thousand cm^{-1}. Where excitation profiles are broad and unresolved, γ is the dominant bandwidth contribution. Homogeneous broadening and inhomogeneous broadening have markedly different effects on the excitation profiles, as illustrated in Figure 3.
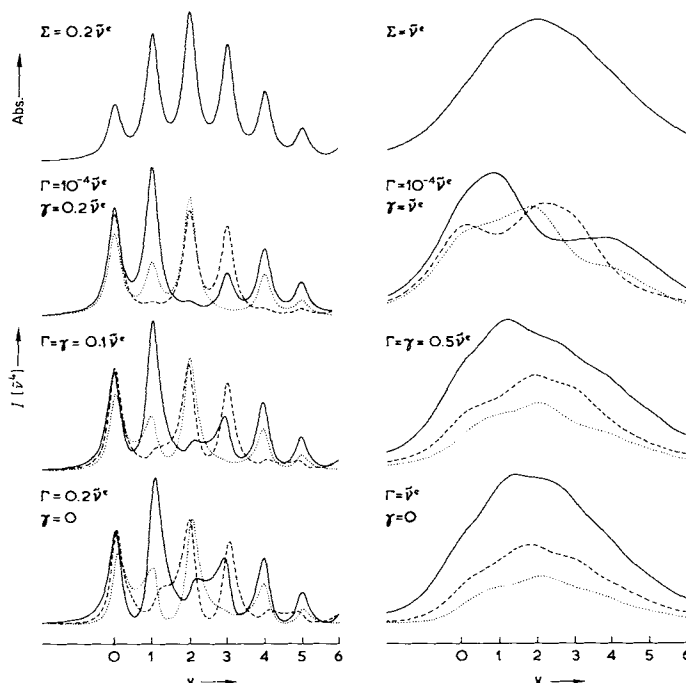

Fig. 3. Top, Absorption spectra, and bottom, resonance Raman excitation profiles (v_1 (——), $2 v_1$ (---) and $3 v_1$ (····) bands) for $\bar{v}^e = \bar{v}^g$, $\Delta = 1.5$ and $\Sigma = 0.2 \bar{v}^e$ or $\bar{v}^e$ (abscissa expressed in terms of excited-state vibrational quanta, v). The excitation profiles are given for $\Gamma/\gamma = \infty$, 1 and ca. 0 (Γ may not be equated to zero because the excitation profile is then indeterminate). Abs = Absorption, I = Raman intensity.

The principal differences are that (a) γ plays no part in the aforementioned interference phenomena, and (b) increasing the Γ contribution (maintaining constant Σ) decreases the intensity of overtones relative to that of the fundamental. By measuring EPs of molecules in different environments (i.e. different solvents or host lattices) it is possible to determine Γ, and hence the excited-state lifetime, since this is largely independent of molecular environment. This information cannot be obtained from absorption spectra because these are insensitive to variation in the relative contributions of Γ and γ, the bandwidths being given by the sum Σ.

So far the treatment has been restricted to molecules with only one totally symmetric mode and for which only one excited state contributes to the transition polarizability. This latter assumption is not justified when two or more (N) excited states are in close proximity to one another, and the transition polarizability must then include the sum of contributions from each state, viz.

$$[\alpha_{\rho\rho}]_{gn,g0} = \frac{1}{hc} \sum_{i=1}^{N} |[\mu_\rho]^0_{ge_i}|^2 \sum_{v_i} \frac{\langle n_g|v_{e_i}\rangle\langle v_{e_i}|0_g\rangle}{\bar{v}_{e_i v} - \bar{v}_0 + i\Gamma_{e_i v}} \tag{22}$$

The Raman intensity is given by

$$I_{gn,g0}(\pi/2) = K(\bar{v}_0 - \bar{v}_{gn,g0})^4 \sum_{i=1}^{N} \sum_{i'=1}^{N} |[\mu_\rho]^0_{ge_i}|^2 |[\mu_\rho]^0_{ge_{i'}}|^2 \times \sum_v \sum_{v'} \langle n_g|v_{e_i}\rangle\langle v_{e_i}|0_g\rangle\langle n_g|v'_{e_{i'}}\rangle\langle v'_{e_{i'}}|0_g\rangle$$

$$\times \left(\frac{[(\varepsilon_v^i - \varepsilon_{v'}^{i'})^2 + (\Gamma_i + \Gamma_{i'})(\Sigma_i + \Sigma_{i'})][\varepsilon_v^i\varepsilon_{v'}^{i'} + \Sigma_i\Sigma_{i'}] - \frac{1}{2}(\varepsilon_v^i - \varepsilon_{v'}^{i'})(\gamma_i + \gamma_{i'})(\Sigma_i + \Sigma_{i'})}{[(\varepsilon_v^i)^2 + \Sigma_i^2][(\varepsilon_{v'}^{i'})^2 + \Sigma_{i'}^2][(\varepsilon_v^i - \varepsilon_{v'}^{i'})^2 + (\Gamma_i + \Gamma_{i'})^2]} \right) \tag{23}$$

In addition to the interferences between vibronic contributions of the same state there are also interferences between the contributions from different states; these arise from the sign differences of ε_v^i values at certain positions and will also occur if Δ is positive for one state but negative for a second. Some examples of interference effects are shown in Figure 4.

The extension of the theory to molecules with several totally symmetric modes is straightforward if it may be assumed that the normal coordinates of the excited state are identical to those of the ground state. The multi-dimensional overlap integrals $\langle \bar{n}_g|\bar{v}_e\rangle$ may then be expressed as products of one-dimensional ones:

$$\langle \bar{n}_g|\bar{v}_e\rangle = \langle (n_1 n_2 n_3 \ldots n_N)_g | (v_1 v_2 v_3 \ldots v_N)_e\rangle = \prod_{i=1}^{N} \langle n_{ig}|v_{ie}\rangle \tag{24}$$

Substitution of these products into either Equation (18) (one-state) or Equation (23) (multi-state) enables excitation profiles to be calculated. By fitting these to experimental data, values for ΔQ_1, ΔQ_2, etc., can be deduced, i.e. the displacement of the excited-state potential minimum along each of the totally symmetric normal coordinates. The relationship between these displacements and the geometric changes attendant upon electronic excitation (bond-length and bond-angle changes) is less straightforward than in the single-mode case. Internal coordinates are related to normal coordinates by the matrix equation

$$\mathbf{R} = \mathbf{L}\mathbf{Q} \tag{25}$$

where $\mathbf{R}$ is a column matrix comprising the $3N-6$ internal coordinates, $\mathbf{Q}$ is a column matrix of the $3N-6$ normal coordinates, and $\mathbf{L}$ is a square matrix effecting the transformation from normal to internal coordinates; it is obtained by solution of the vibrational secular equation. For the states $|g\rangle$ and $|e\rangle$ we may write

$$\mathbf{R}_g = \mathbf{L}_g\mathbf{Q}_g$$

$$\mathbf{R}_e = \mathbf{L}_e\mathbf{Q}_e \tag{26}$$

$$\mathbf{R}_e - \mathbf{R}_g = \mathbf{L}_e\mathbf{Q}_e - \mathbf{L}_g\mathbf{Q}_g \tag{27}$$
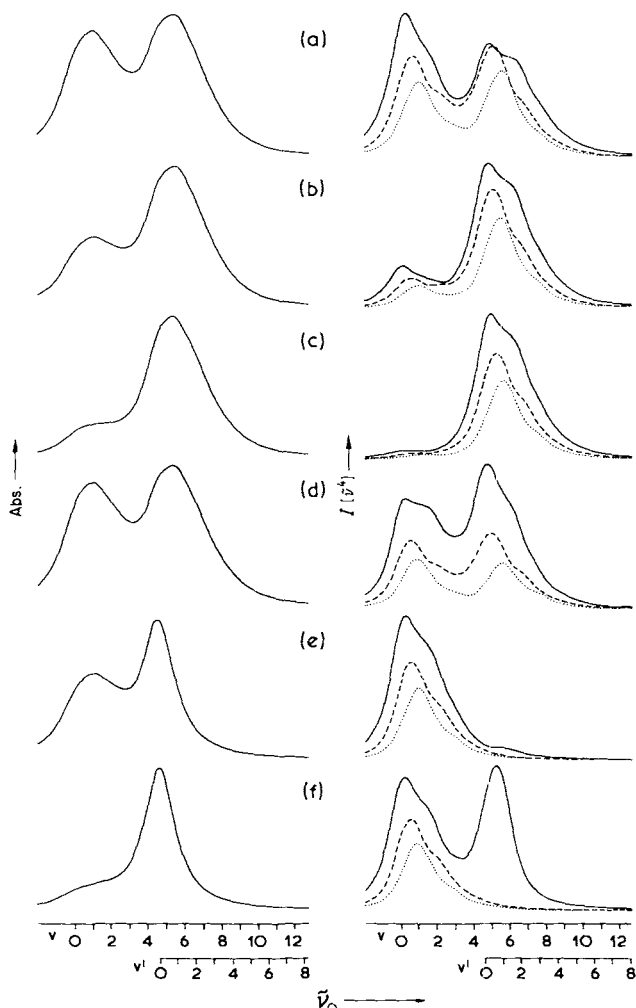

Fig. 4. Absorption spectra and resonance Raman excitation profiles (ν_1 (——), $2\nu_1$ (---), and $3\nu_1$ (····) bands) for a selection of different examples in which two electronic transitions, $|e_1\rangle\leftarrow|g\rangle$ and $|e_2\rangle\leftarrow|g\rangle$, contribute. (a) $R_{12}=1$, $\Delta_1=\Delta_2=1.5$; (b) $R_{12}=2$, $\Delta_1=\Delta_2=1.5$; (c) $R_{12}=5$, $\Delta_1=\Delta_2=1.5$; (d) $R_{12}=1$, $\Delta_1=1.5$, $\Delta_2=-1.5$; (e) $R_{12}=1$, $\Delta_1=1.5$, $\Delta_2=0.1$; (f) $R_{12}=5$, $\Delta_1=1.5$, $\Delta_2=0.1$. $R_{12}=|[\mu_\rho]^0_{ge_2}/[\mu_\rho]^0_{ge_1}|^2$; Δ_1 and Δ_2 are the displacement parameters for the two transitions. The abscissa is expressed in terms of vibrational quanta of the excited states $|e_1\rangle$ (v) and $|e_2\rangle$ (v'), where $\bar{v}^{e_1}=\bar{v}^{e_2}$. Other parameters used in the calculation are $\Delta v_{e_2 e_1}=4.3\,\bar{v}^{e_1}$ and $\Gamma=\gamma=0.5\,\bar{v}^{e_1}$. The observed interference effects are diminished when Γ and γ are made smaller.

By making the assumption that the L matrix is unchanged in the excited state (which is necessary in the absence of a detailed knowledge of the excited-state vibrations), it follows that

$$\mathbf{R}_e - \mathbf{R}_g = \mathbf{L}(\mathbf{Q}_e - \mathbf{Q}_g)$$
$$\text{or } \Delta\mathbf{R} = \mathbf{L}\Delta\mathbf{Q} \tag{28}$$

where $\Delta\mathbf{R}$ is a column matrix of the internal coordinate changes and $\Delta\mathbf{Q}$ is a column matrix of the normal coordinate displacements. We may take advantage of molecular symmetry by recasting this equation in the form

$$\Delta\mathbf{R} = \tilde{\mathbf{U}}\,\mathscr{S}\,\Delta\mathbf{Q} \tag{29}$$

where $\tilde{\mathbf{U}}$ is the transpose of the matrix relating internal coordinates to symmetry coordinates and $\mathscr{S}$ is the symmetrized version of the L matrix. The $\mathscr{S}$ matrix factorizes into a block diagonal form and only the block involving totally symmetric coordinates needs to be considered.

RR spectra of molecules possessing more than one totally symmetric mode may display overtone progressions for each of the active vibrations, i.e. those for which there are normal coordinate displacements. Additionally there may also be combination band progressions involving quanta of more than one mode. In general it is true that the most displaced coordinate will give rise to the greatest intensity enhancement and the longest overtone progression. On this basis it is still possible to make a qualitative assessment of the excited-state geometry from RR data when detailed calculations cannot be performed.

A special case of the A-term scattering regime exists when each of the displacements, ΔQ, is very small but non-zero.[38] In this situation it can be seen from Equations (16) that, assuming $\tilde{v}_i^e = \tilde{v}_i^g$, the overlap integrals have the values

$$\langle 1_g | 1_e \rangle = \langle 0_g | 0_e \rangle = 1$$

$$\langle 1_g | 0_e \rangle = -\langle 0_g | 1_e \rangle = -\Delta$$

Integrals in which either n or v has a value of 2 or more and $n \neq v$ may be approximated to zero because they involve higher powers of Δ ($\Delta \ll 1$ and so $\Delta^2 \ll \Delta$). The summation over the levels v is therefore restricted to the $v = 0$ and $v = 1$ contributions, and Franck-Condon factors will be non-zero only for $n = 0$ (Rayleigh scattering) and $n = 1$ (fundamental Raman scattering). Thus, in the small displacement approximation, overtones are forbidden.

The multi-dimensional Franck-Condon factors may be expressed in the following form:

$$\langle \bar{n}_g | \bar{v}_e \rangle \langle \bar{v}_e | \bar{0}_g \rangle = \langle 1_{ag} | 0_{ae} \rangle \langle 0_{ae} | 0_{ag} \rangle \prod_{i=1}^{m-1} \langle 0_{ig} | v_{ie} \rangle^2 \tag{30}$$

$$\text{or } \langle 1_{ag} | 1_{ae} \rangle \langle 1_{ae} | 0_{ag} \rangle \prod_{i=1}^{m-1} \langle 0_{ig} | v_{ie} \rangle^2$$

Within the framework of the small-displacement approximation the product has the value unity, allowing each vibrational mode to be treated as an independent oscillator.

The excitation profile for the ath fundamental is then given by

$$I_{g1_a,g0} = K(\tilde{v}_0 - \tilde{v}_{g1_a,g0})^4 \,|[\mu_\rho]_{ge}^0|^4 \tag{31}$$

$$\times \Delta_a^2 \frac{\left\{ \frac{\Sigma}{\Gamma}[\varepsilon_0^2 + \varepsilon_1^2 + 2\Sigma^2][(\varepsilon_1 - \varepsilon_0)^2 + 4\Gamma^2] - 2[\varepsilon_0\varepsilon_1 + \Sigma^2][(\varepsilon_0 - \varepsilon_1)^2 + 4\Gamma\Sigma] \right\}}{(\varepsilon_0^2 + \Sigma^2)(\varepsilon_1^2 + \Sigma^2)[(\varepsilon_0 - \varepsilon_1)^2 + 4\Gamma^2]}$$

where Δ_a is the displacement parameter for the ath totally symmetric mode, the wave number of which is $\tilde{v}_a$. Although it is not possible to determine absolute values for the displacement parameters in this approximation, the relative magnitudes (but not signs) may be deduced from the relative intensities of the RR bands. Taking account of molecules initially in $m > 0$ vibrational levels, the relative displacements can be calculated from

$$\frac{|\Delta_a|}{|\Delta_b|} = \left\{ \frac{I_{g1_a,g0}}{I_{g1_b,g0}} \left(\frac{\tilde{v}_0 - \tilde{v}_b}{\tilde{v}_0 - \tilde{v}_a} \right)^4 \left(\frac{1 - \exp(-hc\tilde{v}_a/kT)}{1 - \exp(-hc\tilde{v}_b/kT)} \right) \frac{\tilde{v}_b^2}{\tilde{v}_a^2} \right\}^{1/2} \tag{32}$$

As pointed out earlier, B-term scattering may occur for totally symmetric modes if the excited states $|e\rangle$ and $|s\rangle$ are of the same symmetry. B-term excitation profiles for totally symmetric modes are given by

$$I_{g1_a,g0} = K\,|[\mu_\rho]_{ge}^0|^2\,|[\mu_\rho]_{gs}^0|^2 \left(\frac{h_{es}^a}{\Delta\tilde{v}_{es}} \right)^2 (\tilde{v}_0 - \tilde{v}_{g1_a,g0})^4 \tag{33}$$

$$\times \frac{\left\{ \frac{\Sigma}{\Gamma}[\varepsilon_0^2 + \varepsilon_1^2 + 2\Sigma^2][(\varepsilon_1 - \varepsilon_0)^2 + 4\Gamma^2] + 2[\varepsilon_0\varepsilon_1 + \Sigma^2][(\varepsilon_0 - \varepsilon_1)^2 + 4\Gamma\Sigma] \right\}}{(\varepsilon_0^2 + \Sigma^2)(\varepsilon_1^2 + \Sigma^2)[(\varepsilon_0 - \varepsilon_1)^2 + 4\Gamma^2]}$$

The wave-number-dependent part of this expression differs from that of Equation (31) in that the second term in the numerator is positive rather than negative. This may result in destructive interference between the 0-0 and 0-1 maxima and constructive interference elsewhere, the opposite being true for the A-term. Figure 5 shows examples of B-term and small-displacement A-term excitation profiles, while Figure 6 shows the effect of A-term/B-term interference; this occurs when the two terms have similar magnitudes.[45] The interference is constructive for the 0-0 resonance and destructive for the 0-1 resonance, but this behavior is reversed if the transition moments $[\mu_\rho]_{ge}^0$ and $[\mu_\rho]_{gs}^0$ have opposite signs. Similar excitation profiles may result if there is non-adiabatic coupling of the states $|e\rangle$ and $|s\rangle$ (vide infra).

2.4. Resonance Raman Scattering Involving Non-Totally Symmetric Modes

RR bands attributed to non-totally symmetric fundamental vibrations may acquire intensity via one of three scattering mechanisms:

(1) A-term activity due to a change of molecular symmetry in the resonant excited-state;
(2) A-term activity due to excited-state JT coupling;
(3) B-term scattering, involving the vibronic coupling of the resonant state to a second electronic excited state.
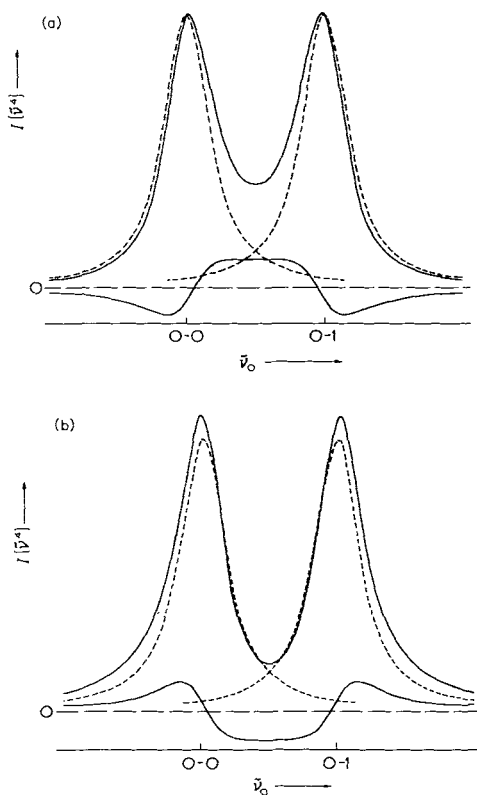
138

Fig. 5. Excitation profiles for (a) small displacement A-term scattering, and (b) B-term scattering, showing the 0-0 and 0-1 contributions (---) and the interference contribution (——) to the Raman intensity I, calculated with $\Gamma = \gamma = 0.1\,\bar{\nu}^c$.
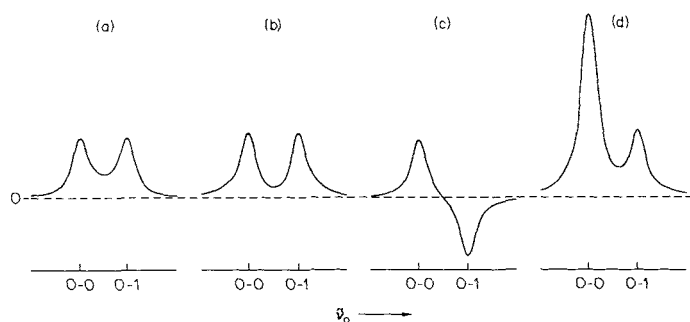

Fig. 6. Excitation profile (d) for A-term/B-term interference showing (a) the A-term, (b) B-term, and (c) interference contributions to the Raman intensity for the case where the A-term and B-term are equal. The calculations were obtained with $\Gamma = \gamma = 0.1\,\bar{\nu}^c$, and only small changes occur when Γ/γ is varied.

If a molecule undergoes a change of symmetry upon excitation then the A-term active modes are those that are totally symmetric in the subgroup formed by the symmetry operations common to the ground- and excited-state point groups (common group). A good example is provided by the molecule ethylene which has a planar D_{2h} geometry in the ground state and a twisted D_{2d} geometry in the first $^1B_{1u}$ excited state. The common group is D_2 and, by correlation of D_2 to D_{2h}, it is seen that the A-term active modes are those of a_g and a_u symmetry. Of course the a_u fundamental (v_7, the twist about the C=C bond) is Raman inactive but even quanta thereof, i.e. $2v_7$, $4v_7$, etc., have A_g

symmetry and are accordingly Raman active. Excitation within the contour of the π-π^* transition of ethylene using 193.4 nm irradiation[46] yields RR spectra displaying progressions in the $v(C=C)$ mode and even harmonics of $v_7(a_u)$. This recent study thus provided the first unambiguous evidence for a twisted excited state for ethylene. It is a general empirical rule that the vibrational coordinates responsible for converting a molecule from its ground- to excited-state geometry will give rise to resonance-enhanced Raman bands (Tsuboi's rule[47]).

In cases where the resonant excited state is degenerate, A-term activity may arise for some non-totally symmetric modes. The non-totally symmetric vibrations belonging to the irreducible representations contained in the symmetric direct product $\{\Gamma_e \otimes \Gamma_e\}$ may be responsible for JT coupling in the excited state. Some common examples of excited states so influenced are $T_2(T_d)$, $T_{1u}(O_h)$ and $E_u(D_{4h})$, for which the direct products are as follows:

$$T_2 \otimes T_2 = \{A_1 + E + T_2\} + [T_1]$$
$$T_{1u} \otimes T_{1u} = \{A_{1g} + E_g + T_{2g}\} + [T_{1g}]$$
$$E_u \otimes E_u = \{A_{1g} + B_{1g} + B_{2g}\} + [A_{2g}]$$

Vibrations transforming as the antisymmetric part of the direct product (given in square brackets) are not JT active because they do not lift the degeneracy of the excited state. This point is best illustrated by reference to an ion belonging to the D_{4h} point group, e.g. in Figure 7 is shown the effect of vibrations of b_{1g}, b_{2g} and a_{2g} symmetry for the square planar $[Pt(CN)_4]^{2-}$ ion. It is evident that, whereas b_{1g} and b_{2g} vibrations remove the C_4-axis (which is responsible for the double degeneracy), an a_{2g} vibration does not; thus the b_{1g} and b_{2g} modes, but not the a_{2g} mode, are JT active.

The effect of excited-state JT effects on RR spectra may be summarized as follows:

(1) The appearance of combination band progressions involving quanta of totally symmetric modes plus one quantum of a JT-active vibration (small JT effect);

(2) the appearance of combination band progressions involving quanta of totally symmetric modes plus multiple quanta of JT-active vibrations, as well as overtone progressions of the latter (strong JT effect).
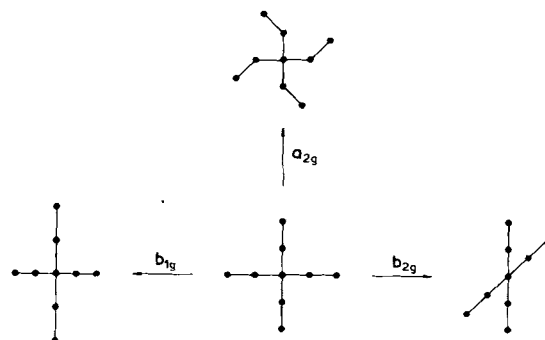

Fig. 7. Diagram showing the effect of a_{2g}, b_{1g} and b_{2g} distortions on a D_{4h} species, e.g. $[Pt(CN)_4]^{2-}$.

139

It is to be expected that the excited-state JT effect is a dynamic one and that no permanent distortion of the molecule occurs. Thus the major geometric changes accompanying excitation to a degenerate excited state are those involving totally symmetric modes and case (2) is something of a rarity.

For many polyatomic molecules B-term scattering is the major source of RR activity for non-totally symmetric modes. As pointed out earlier, its magnitude is dependent on the vibronic coupling integral h_{es}^k. It is therefore necessary that, for a non-totally symmetric coordinate Q_k to be B-term active, it must be effective in coupling the resonant state $|e\rangle$ to a second excited state $|s\rangle$. Expressed group theoretically, Γ_k must be contained in the product $\Gamma_e \otimes \Gamma_s$. From Equation (14) the transition polarizability is given by

$$[\alpha_{\rho\sigma}]_{g1,g0} = \frac{1}{h^2 c^2} [\mu_\rho]_{gs}^0 [\mu_\sigma]_{eg}^0 \frac{h_{se}^k}{\Delta\bar{\nu}_{es}} \langle 1|Q_k|0\rangle (\varepsilon_0 + i\Gamma)^{-1}$$
$$+ \frac{1}{h^2 c^2} [\mu_\rho]_{ge}^0 [\mu_\sigma]_{sg}^0 \frac{h_{es}^k}{\Delta\bar{\nu}_{es}} \langle 1|Q_k|0\rangle (\varepsilon_1 + i\Gamma)^{-1}$$

(34)

where $\langle 1|Q_k|0\rangle = \langle 1_e|Q_k|0_g\rangle = \langle 1_g|Q_k|0_e\rangle$

Close examination of this expression reveals that $\alpha_{\rho\sigma} \neq \alpha_{\sigma\rho}$, i.e. that the polarizability tensor is asymmetric. The latter may be expressed as the sum of symmetric and antisymmetric tensors, viz.

$$\alpha_{\rho\sigma} = \left(\frac{\alpha_{\rho\sigma} + \alpha_{\sigma\rho}}{2}\right) + \left(\frac{\alpha_{\rho\sigma} - \alpha_{\sigma\rho}}{2}\right)$$

(35)

where the matrix elements are given by

$$[\alpha_{\rho\sigma}]_{g1,g0} \pm [\alpha_{\sigma\rho}]_{g1,g0} = \frac{1}{h^2 c^2} \frac{h_{es}^k}{\Delta\bar{\nu}_{es}} \langle 1|Q_k|0\rangle$$
$$\times \{[\mu_\rho]_{gs}^0 [\mu_\sigma]_{eg}^0 + [\mu_\rho]_{ge}^0 [\mu_\sigma]_{sg}^0\} \left(\frac{1}{\varepsilon_0 + i\Gamma} \pm \frac{1}{\varepsilon_1 + i\Gamma}\right)$$

(36)

Excitation profiles for Raman bands involving symmetric (+) and antisymmetric (−) tensor contributions are given by

$$I_{g1,g0}^{(\pm)} = K \frac{\left\{\frac{\Sigma}{\Gamma}[\varepsilon_0^2 + \varepsilon_1^2 + 2\Sigma^2][(\varepsilon_1 - \varepsilon_0)^2 + 4\Gamma^2] \pm 2[\varepsilon_0\varepsilon_1 + \Sigma^2][(\varepsilon_0 - \varepsilon_1)^2 + 4\Gamma\Sigma]\right\}}{(\varepsilon_0^2 + \Sigma^2)(\varepsilon_1^2 + \Sigma^2)[(\varepsilon_0 - \varepsilon_1)^2 + 4\Gamma^2]}$$

(37)

The antisymmetric tensor EP resembles that arising from the small displacement A-term, i.e. there is constructive interference between the 0-0 and 0-1 resonances and destructive interference elsewhere. Thus, the antisymmetric tensor contribution becomes zero outside of the resonance region and normal, i.e. off-resonance, vibrational Raman scattering is controlled exclusively by a symmetric polarizability tensor. By contrast, electronic Raman transitions can involve antisymmetric scattering even in the off-resonance case. The most notable observations of antisymmetric scattering by non-totally symmetric modes have been for metalloporphyrin systems. Resonance Raman spectra obtained by excitation within the Q-band (E_u symmetry) are

dominated by B-term scattering by vibrations which couple the Q-state to the higher energy Soret state (also of E_u symmetry). The B-term active vibrations are given by

$$E_u \otimes E_u = A_{1g} + A_{2g} + B_{1g} + B_{2g}$$

and the antisymmetric part of the product, A_{2g}, gives rise to antisymmetric scattering. Weak overtones of a_{1g}, a_{2g}, b_{1g}, and b_{2g} modes are sometimes observed in metalloporphyrin RR spectra and represent the only known examples of D-term scattering.

In concluding this section it should be pointed out that two complications may arise:

(1) Interference between contributions to the transition polarizability from JT-activity (intramanifold coupling) and B-term activity (intermanifold coupling);
(2) Non-adiabatic coupling, which may arise when the states $|e\rangle$ and $|s\rangle$ are close together, i.e. when $\Delta\bar{\nu}_{es}$ is comparable with vibrational band wave numbers.[48]

The effect of either of these two processes is that the 0-0 and 0-1 peaks in the excitation profiles display unequal intensities. Modes of a_{2g} symmetry are JT inactive and show only the non-adiabatic effect, which favors the 0-1 resonance. This contrasts with the behavior of the other modes which tend to produce stronger 0-0 scattering, arising from interference between the inter- and intramanifold contributions.

2.5. Depolarization Ratios

The depolarization ratio for 90° Raman scattering excited by linearly polarized incident radiation (see Fig. 8) is given by

$$\rho(\pi/2) = \frac{^\perp I_\parallel (\pi/2)}{^\perp I_\perp (\pi/2)}$$

(38)

where $\perp$ and $\parallel$ are defined by reference to the scatter plane (the plane containing the directions of propagation of the incident and scattered radiation) and the superscripts and subscripts refer to incident and scattered polarizations, respectively. For an assembly of randomly orien-
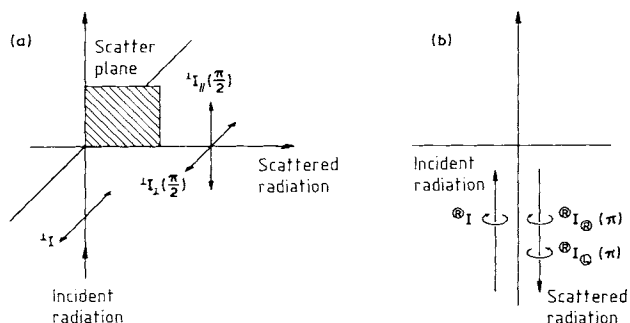

Fig. 8. The geometry for scattering at (a) 90° using linearly polarized incident radiation, and (b) 180° using circularly polarized incident radiation.

tated molecules $\rho(\pi/2)$ may be expressed in terms of the tensor invariants $\bar{\alpha}$, γ_s, and γ_{as} thus:

$$\rho(\pi/2) = \frac{3\gamma_s^2 + 5\gamma_{as}^2}{45\bar{\alpha}^2 + 4\gamma_s^2} \qquad (39)$$

where

$$\gamma_s^2 = \tfrac{1}{2}\{(\alpha_{xx} - \alpha_{yy})^2 + (\alpha_{yy} - \alpha_{zz})^2 + (\alpha_{zz} - \alpha_{xx})^2 + \tfrac{3}{2}[(\alpha_{xy} + \alpha_{yx})^2 + (\alpha_{yz} + \alpha_{zy})^2 + (\alpha_{zx} + \alpha_{xz})^2]\}$$

$$\gamma_{as}^2 = \tfrac{3}{4}[(\alpha_{xy} - \alpha_{yx})^2 + (\alpha_{yz} - \alpha_{zy})^2 + (\alpha_{zx} - \alpha_{xz})^2]$$

For vibrational non-RR scattering γ_{as}^2 is zero, because, as stated previously, the antisymmetric polarizability tensor vanishes under these conditions. The following behavior is then observed:[49]

(1) For non-totally symmetric modes only off-diagonal polarizability tensor elements, $\alpha_{\rho\sigma}$, and the combination $(\alpha_{xx} - \alpha_{yy})$ are non-zero. Therefore $\bar{\alpha} = 0$ for all non-totally symmetric modes and $\rho(\pi/2) = 3/4$;

(2) for cubic molecules $\alpha_{xx} = \alpha_{yy} = \alpha_{zz}$, hence $\gamma_s^2 = 0$ for totally symmetric modes and $\rho(\pi/2) = 0$. Both $\bar{\alpha}$ and γ_s^2 may be non-zero for the totally symmetric modes of non-cubic molecules and $0 \leqslant \rho(\pi/2) \leqslant 3/4$.

Depolarization ratios for RR scattering are determined by the symmetry of the resonant transition and can provide a valuable tool for the determination of electronic band assignments. For totally symmetric modes of molecules not belonging to the point groups C_1, C_i, C_s, C_2 or C_{2h}, only the diagonal polarizability components, $\alpha_{\rho\rho}$, are non-zero. If the resonant transition is non-degenerate then only one of these will be non-zero (say α_{xx} if the transition is x-polarized) and, from Equations (39), $\rho(\pi/2) = 1/3$. Similarly, it can be shown that a doubly-degenerate resonant transition (x,y-polarization) gives rise to $\rho(\pi/2) = 1/8$, and that a cubic molecule for which only triply-degenerate transitions are electric-dipole-allowed (x,y,z-polarization), $\rho(\pi/2) = 0$. Two further cases may arise when either two non-degenerate transitions lie close together or when a non-degenerate transition is in close proximity to a doubly-degenerate one. In the former case the $\rho(\pi/2)$ value will depend on the relative magnitudes of, say α_{xx} and α_{yy}, illustrated in Figure 9, and will vary as functions of the excitation wave number $\tilde{v}_0$ (polarization dispersion). Likewise, in the second case the $\rho(\pi/2)$ value will depend on the relative magnitudes of say $\alpha_{xx} = \alpha_{yy}$ and α_{zz}; this situation is shown in Figure 10.

If the molecular point group is either C_1, C_i, C_s, C_2 or C_{2h} then off-diagonal components, $\alpha_{\rho\sigma}$, may also be non-zero if B-term scattering occurs. Thus, the $\rho(\pi/2)$ is most likely to be within the range 0 to 3/4.

Departure from the above-mentioned behavior is expected if the electronic ground state is degenerate, for then the Raman transition is not a purely vibrational one. The Raman transition is $|g\rangle|n\rangle \leftarrow |g\rangle|0\rangle$, in the low temperature limit, and the irreducible representation for this process is given by $\Gamma_g \otimes \Gamma_n \otimes \Gamma_g \otimes \Gamma_1$ (the $v = 0$ level is necessarily totally symmetric). It is clear that, for a non-degenerate ground state, the product is simply Γ_n because $\Gamma_g \otimes \Gamma_g = \Gamma_1$. However, it is equally clear that if the ground state is de-
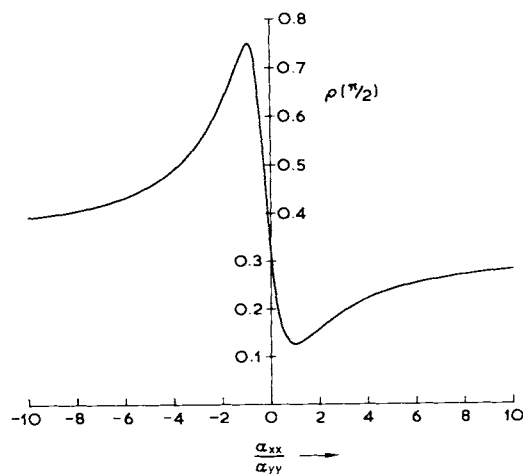

Fig. 9. Plot of $\rho(\pi/2)$ versus α_{xx}/α_{yy} for the case in which two non-degenerate transitions contribute to the transition polarizability.
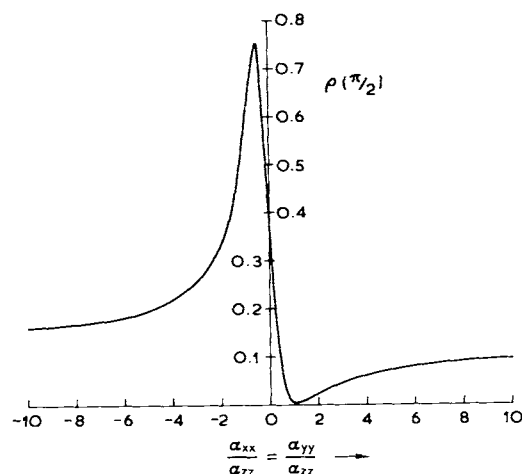

Fig. 10. Plot of $\rho(\pi/2)$ versus $\alpha_{xx}/\alpha_{zz} = \alpha_{yy}/\alpha_{zz}$ for the case in which one degenerate and one non-degenerate transition contribute to the transition polarizability.

generate then this will affect the symmetry of the transition. As an example, consider a doubly degenerate E_g'' ground state of an octahedral molecule (O_h point group). The product $E_g'' \otimes E_g'' = A_{1g} + T_{1g}$, and thus the Raman bands attributed to $v_1(a_{1g})$ and its overtones will transform as $A_{1g} + T_{1g}$. Both $\bar{\alpha}$ and γ_{as}^2 will be non-zero and $\rho(\pi/2)$ may take any value between zero and infinity, depending on the relative magnitudes of $\bar{\alpha}$ and γ_{as}^2, and will show dispersion throughout the resonance region. Such behavior has been observed for $[IrBr_6]^{2-}$ and $[IrCl_6]^{2-}$,[50] where the ground state is the E_g'' spin-orbit component of the $^2T_{2g}$ term.

If the ground state is orbitally non-degenerate but possesses spin degeneracy then strong spin-orbit coupling may cause mixing of the ground state with degenerate excited states of the same spin degeneracy. Thus, the ground state acquires some degenerate character and the depolarization ratios of totally symmetric modes may become anomalously large. The only reported observation of this is for $[FeBr_4]^-$ where spin-orbit coupling causes the $^6A_1$ ground state to be mixed with sextet excited states, and $\rho(\pi/2) = 0.15$ is observed for the v_1 band in the RR spectrum.[51,52]

Angew. Chem. Int. Ed. Engl. 25 (1986) 131–158

141

$$\rho(\pi/2) = \frac{3}{4} + \frac{5}{4}\frac{\gamma_{as}^2}{\gamma_s^2} = \frac{3}{4} + \frac{5}{4}\left|\frac{[\alpha_{\rho\sigma}]_{gn,g0} - [\alpha_{\sigma\rho}]_{gn,g0}}{[\alpha_{\rho\sigma}]_{gn,g0} + [\alpha_{\sigma\rho}]_{gn,g0}}\right|^2 = \frac{3}{4} + \frac{5}{4}\frac{\left\{\frac{\Sigma}{\Gamma}[\varepsilon_0^2 + \varepsilon_1^2 + 2\Sigma^2][(\varepsilon_1 - \varepsilon_0)^2 + 4\Gamma^2] - 2[(\varepsilon_1 - \varepsilon_0)^2 + 4\Gamma\Sigma][\varepsilon_1\varepsilon_0 + \Sigma^2]\right\}}{\left\{\frac{\Sigma}{\Gamma}[\varepsilon_0^2 + \varepsilon_1^2 + 2\Sigma^2][(\varepsilon_1 - \varepsilon_0)^2 + 4\Gamma^2] + 2[(\varepsilon_1 - \varepsilon_0)^2 + 4\Gamma\Sigma][\varepsilon_1\varepsilon_0 + \Sigma^2]\right\}} \tag{40}$$

For non-totally symmetric modes $\bar{\alpha}$ is zero and the $\rho(\pi/2)$ value is dependent on the relative sizes of γ_s^2 and γ_{as}^2. If, for a given symmetry class, there are only symmetric or antisymmetric tensor components, then $\rho(\pi/2) = 3/4$ or ∞, respectively, and does not display dispersion. Examples of such vibrational modes are the b_{1g} and b_{2g} modes (symmetric tensor) and a_{2g} modes (antisymmetric tensor) of metalloporphyrins. By contrast, for cases in which both symmetric and antisymmetric tensor components transform as the same irreducible representation (e.g. B_{1g}, B_{2g} or B_{3g} in the D_{2h} point group), $\rho(\pi/2)$ lies between 3/4 and ∞ and displays dispersion throughout the resonance region. The variation of $\rho(\pi/2)$ with excitation wave number [Equation (40)] is readily obtained from Equations (37) and (39). The depolarization ratio $\rho(\pi/2)$ maximizes at the midpoint between the 0-0 and 0-1 resonances and decreases asymptotically towards 3/4 on either side. Its maximum value is a function of Γ and γ, as shown in Figure 11.
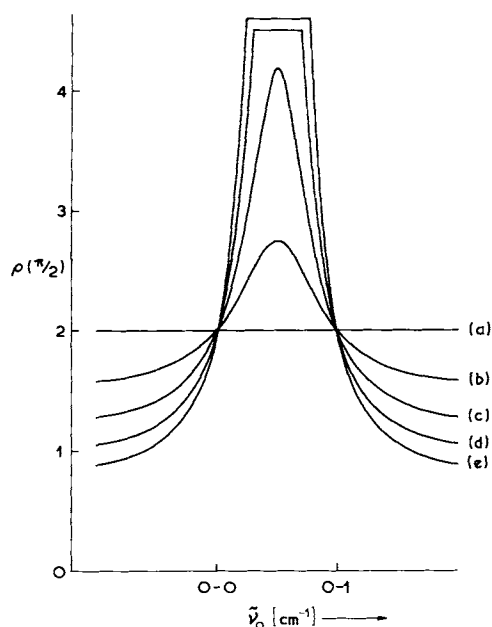

Fig. 11. Polarization dispersion for mixed symmetric/antisymmetric B-term scattering. (a) $\Gamma = 10^{-4}\bar{\nu}^e$, $\gamma = 0.1\bar{\nu}^e$; (b) $\Gamma = 0.025\bar{\nu}^e$, $\gamma = 0.075\bar{\nu}^e$; (c) $\Gamma = \gamma = 0.05\bar{\nu}^e$; (d) $\Gamma = 0.075\bar{\nu}^e$, $\gamma = 0.025\bar{\nu}^e$; (e) $\Gamma = 0.1\bar{\nu}^e$, $\gamma = 0$.

The overtones of non-degenerate non-totally symmetric modes all transform as the totally symmetric representation and their $\rho(\pi/2)$ values will be the same as for totally symmetric fundamentals. Overtones of degenerate fundamentals transform as the symmetric part of the direct product (e.g. in the O_h point group $\{E_g \otimes E_g\} = A_{1g} + E_g$ and $\{T_{2g} \otimes T_{2g}\} = A_{1g} + E_g + T_{2g}$). $\rho(\pi/2)$ values for the overtones of degenerate vibrations have been determined by *Pawlikowski* and *Zgierski*.[53]

An alternative method of investigating the polarization properties of RR scattering involves the use of circularly polarized incident radiation and a 180° scattering geometry, as shown in Figure 8. The quantities that are deter-

mined are the reversal ratio, $\mathscr{P}(\pi)$, which is the ratio of the intensity of contra-rotating to that of co-rotating scattered light, and the degree of circularity, $\mathscr{C}(\pi)$, of the scattered light:

$$\mathscr{P}(\pi) = \frac{^{\otimes}I_{\bigcirc}(\pi)}{^{\otimes}I_{\circledR}(\pi)} = \frac{^{\bigcirc}I_{\circledR}(\pi)}{^{\bigcirc}I_{\bigcirc}(\pi)}$$
$$= \frac{45\bar{\alpha}^2 + \gamma_s^2 + 5\gamma_{as}^2}{6\gamma_s^2} \tag{41}$$

$$^{\otimes}\mathscr{C}(\pi) = \frac{^{\otimes}I_{\circledR}(\pi) - ^{\otimes}I_{\bigcirc}(\pi)}{^{\otimes}I_{\circledR}(\pi) + ^{\otimes}I_{\bigcirc}(\pi)} = -^{\bigcirc}\mathscr{C}(\pi)$$
$$= \frac{45\bar{\alpha}^2 - 5\gamma_s^2 + 5\gamma_{as}^2}{45\bar{\alpha}^2 + 7\gamma_s^2 + 5\gamma_{as}^2} \tag{42}$$

The measurement of Raman spectra excited with both circularly and linearly polarized radiation permits the determination of all three tensor invariants, and so-called "complete" polarization measurements have been carried out for a number of molecules.[54-58] Furthermore, it has recently been shown that meaningful circular polarization measurements can be obtained from samples dispersed in alkali halide disks.[59]

Using the information presented in this section in conjunction with point group tables it is possible for the reader to determine the depolarization ratio, under resonance conditions, for a vibration of any type in any point group. A tabulation of $\rho(\pi/2)$ values for the symmetry classes of all the common point groups is given in Ref. [1].

3. Experimental Techniques

The apparatus required for the excitation, dispersion and detection of RR scattering is precisely the same as that used for normal Raman spectroscopy, although sample illumination procedures are more critical. In order that RR spectroscopy may be applied to a wide range of molecules it is necessary that laser excitation throughout the visible and near UV spectral regions be available. Most RR studies to date have involved excitation provided by CW argon-ion and krypton-ion lasers and CW dye lasers, the latter providing continuously tunable radiation from 395 to 800 nm with seven different dyes (stilbene 1, stilbene 3, coumarin 30, sodium fluorescein, rhodamine 6G, rhodamine 101, and LD 700). Unfortunately, ion lasers provide only a small number of lines in the near-UV (330-370 nm), so it has been necessary to use different laser sources in order to obtain tunable radiation down to 250 nm. At the time of writing, three systems are in current use:

(1) Frequency-doubled output of a mode-locked ion or dye laser. With a repetition rate of ca. 40 MHz the radiation is quasi-CW, but only modest average power can be obtained (ca. 10-20 mW);

(2) Frequency-narrowed excimer lasers and excimer-pumped dye lasers. These have a repetition rate of ca. 10 Hz and average power of the order of 1–10 W; they are, however, very expensive;

(3) Frequency-tripled and -quadrupled pulsed Nd:YAG lasers which may be used to pump a dye laser. Such systems have found considerable application in time-resolved resonance Raman (TR^3) studies.

For most RR studies the scattered light is detected by photomultiplier tubes using photon-counting methods, in many cases employing dedicated computers which also control the spectrometer. In recent years many experiments have been performed using multichannel detection involving either a TV camera (intensifier-vidicon) or diode array. Multichannel detection reduces the time required to obtain a spectrum by several orders of magnitude, thus permitting RR studies of photochemically labile species. In combination with picosecond pulsed lasers, multichannel detection facilitates TR^3 experiments in which transient species and molecules in optically (or radiolytically) pumped excited states may be investigated.[8]

Sample illumination procedures present certain problems associated with strong absorption of the laser beam. These are:

(1) The need for optimization of the concentration of the scattering species in order to achieve a compromise between absorption and scattering processes. Experience has shown that the optimum concentration is best determined experimentally by trial-and-error, but several attempts have been made to calculate optimum sample concentrations for a wide variety of different scattering geometries;

(2) the avoidance of overheating the sample at the laser focus. Various rotating cells for solids, liquids, and gases have been employed and some workers have used devices which enable the focused laser beam to be swept over the sample in a linear or circular fashion. Recently, the use of flowing samples for TR^3 studies has been described;[8]

(3) The elimination of photolysis and luminescence. These can now be discriminated against by the TR^3 techniques mentioned above. Luminescence rejection can be achieved by using single-channel spectrometers in conjunction with pulsed lasers by time-adjusted gating of the photon-counting electronics.

Profound advantages accrue from measuring RR spectra of samples maintained at low temperature, viz. that of minimizing hot-band contribution to intensities and of alleviating thermolysis. This procedure results in a sharpening of the spectral features, thereby improving resolution and signal-to-noise ratios. Several cryostats are available for Raman studies, the most popular being those in which liquid nitrogen (77 K) or liquid helium (4 K) are used as coolants, and also closed-cycle helium gas cryostats (10–12 K). The latter are widely used for matrix-isolation studies.

4. Resonance Raman Studies of Small Molecules

4.1. Diatomic Molecules

Diatomic species (both neutral and ionic) have been subjected to some of the most detailed RR investigations during the last two decades. While many of the earlier studies were concerned with stable species, such as halogen and interhalogen molecules and ions, more recent work has centered on studies of matrix-isolated diatomic metal species. Data on the latter are summarized in Table 2, that on the former being included in earlier tabulations.[1,23]

Recent investigations of the halogens have been concerned with the theoretical interpretation of the spectra of Br_2[77–79] and Cl_2.[80–82] Whereas RR scattering from I_2 can be accounted for by assuming that the transition polarizability is dominated by a single electronic state, $^3\Pi_{0u}^+$ (see Ref. [1] and references therein), scattering from Br_2 contains a contribution from the repulsive $^1\Pi_{1u}$ state. A theoretical study of the EPs[79] has clearly demonstrated the involvement of both states in the scattering process. The theoretical model took account of interference between these contributions but assumed negligible coupling between the two states; this might be an unjustified assumption because the agreement between theory and experiment is poor in the 19 500–21 000 cm^{-1} region. The RR behavior of Cl_2 is quite different in that there seems to be no contribution from the $^3\Pi_{0u}$ state. A RR spectrum displaying an eight-membered progression is observed for 363.8-nm excitation within the contour of the $^1\Pi_{1u} \leftarrow {}^1\Sigma_g^+$ absorption band. However, the intensity enhancement factor of the fundamental for UV excitation with respect to visible, i.e. non-resonant, excitation is only 1.3, and the intensity of the first overtone is only 1/3 of that of the fundamental. These observations have been explained in terms of non-resonant contributions to the polarizability from higher energy states, especially a $^1\Sigma_u^+$ state at 78 500 cm^{-1}. The reason for the absence of a $^3\Pi_{0u}^+$ contribution for Cl_2 is that the transition to this state is spin-forbidden. Its contribution to the RR scattering of Br_2 and, to a greater extent, to that of I_2, obtains from the induction of allowed character into the $^3\Pi_{0u}^+ \leftarrow {}^1\Sigma_g^+$ transition via spin-orbit coupling (this increases in the order Cl < Br < I).

Recent developments in the RR spectroscopy of matrix-isolated metal dimers are of special interest because they provide valuable experimental data upon which to test quantum-chemical calculations. An example of RR scattering by a metal dimer is shown in Figure 12 and Table 1 lists the results obtained so far on diatomic species, although many other metal dimers have been characterized by luminescence spectroscopy.[65] The occurrence of luminescence for some regions of excitation has precluded the more extensive application of RR spectroscopy and renders difficult the measurement of excitation profiles. It is to be hoped that these problems may be overcome in the near future in order that the theoretical interpretation of the spectra may proceed. In particular, it is noted that no unambiguous electronic band assignments have yet been proposed for metal dimers.

Table 2. Resonance Raman data on diatomic species. λ_{max} = wavelength of the electronic band, λ_0 = wavelength of the excitation radiation, ω_e = harmonic wave number, x_e = anharmonicity constant.

Species	State	Electronic band assignment	λ_{max} [nm]	λ_0 [nm]	ω_e [cm^{-1}]	$\omega_e x_e$ [cm^{-1}]	Comments	Ref.
Bi$_2$	Kr matrix, 8 K	A←X	560	568.2	172.7	0.35		[60, 61]
	Ar matrix, 10 K			555	174.3	0.39	Molecular constants obtained from luminescence spectrum superimposed on Raman spectrum	
Br$_2^-$	aq. soln. 295 K	$^2\Sigma_g^+\leftarrow{}^2\Sigma_u^+$	360	355	187.2	−5.17		[62]
Ca$_2$	Kr matrix, 12 K	$^1\Sigma_u^+\leftarrow{}^1\Sigma_g^+$	664	647.1	80	0.35	Ca$_2$ is a van der Waals dimer in the ground state. The excited state is more strongly bound ($\omega_e = 117$ cm^{-1})	[63, 64]
Cl$_2^-$	aq. soln. 295 K	$^2\Sigma_g^+\leftarrow{}^2\Sigma_u^+$	345	355	286.4	−3.83		[62]
Cr$_2$	Ar matrix, 12–15 K			514.5	427.5	15.75		[65]
^{56}Fe$_2$	Ar, Kr matrices, 11 K			457.9	299.6	1.4	The observation of a four-membered anti-Stokes progression is ascribed to radiative population due to long vibrational lifetimes	[66]
FeNi	Ar, Kr matrices, 11 K			457.9	320.0	1.32		[67]
Mn$_2$	Ar matrix, 12–15 K		650	676.4	124.69	0.24	Two electronic Raman bands observed at 135.7 and 196.7 cm^{-1}	[67]
Pb$_2$	Kr, Xe matrices, 8–10 K	FO$_u^+\leftarrow$XO$_g^+$	515	476.2, 647.1	110	0.75		[68]
	Xe matrix, 12 K			496.5	108	0.4		[69]
	Ar, Ne matrices, 8–10 K			514.5	110 (Ne), 112.2 (Ar)	0.35	In Ar matrices a second strong progression is observed ($\omega_e = 123$, $\omega_e x_e = 0.26$ cm^{-1}) assigned to Raman scattering from the electronic excited A state at ca. 5500 cm^{-1}	[70]
S$_2^-$	Ultramarine green lattice	$^2\Pi_g\leftarrow{}^2\Pi_u$	393	406.7	597.0	2.5±0.15	$\rho\left(\frac{\pi}{2}\right) = 0.14\pm0.03$ for fundamental of species in solution (Na$_2$S$_4$/DMF) confirms that transition is x,y-polarized. $\Delta r = 0.30\pm0.01$ Å, $\Gamma = 300\pm50$ cm^{-1} and $\gamma = 400\pm50$ cm^{-1} [a, b]	[71, 72]
Sc$_2$	Ar matrix, 12–15 K			676.4	238.91	0.93		[67]
Se$_2^-$	Ultramarine selenium, 80 K	$^2\Pi_g\leftarrow{}^2\Pi_u$	490	488.0	329.6±0.3	0.70±0.03	$\Delta r = 0.32\pm0.02$ Å, $\Gamma = 150\pm50$ cm^{-1} and $\gamma = 400\pm100$ cm^{-1} [b]	[72]
Sn$_2$	Ar matrix, 12 K		490	488.0	188	0.53		[73, 74]
Ti$_2$	Ar matrix, 11 K			632.8	407.9	1.08	Anti-Stokes progression also observed, implying long vibrational lifetimes	[75]
V$_2$	Ar matrix, 11 K			488.0	537.5	4.2	Anti-Stokes progression. Three other Stokes progressions observed, assigned to electronic Raman and scattering from an excited state	[75]
Xe$_2^+$	[SbF$_6$]$^-$ salt in SbF$_5$ solution	$^2\Pi_{1/2g}\leftarrow{}^2\Sigma_u^+$	710	676.4	123	0±1	Isoelectronic with I$_2^-$	[76]

[a] DMF = dimethylformamide. [b] Obtained from calculations of excitation profiles.

One aspect of these studies that deserves mention concerns the observation of anti-Stokes overtone progressions in Ca$_2$, Fe$_2$, Ti$_2$, and V$_2$. These cannot arise from thermal population of vibrational levels of the ground state because, at ca. 10 K, all molecules must be in the v = 0 level. The effect has been attributed to population of the v > 0 levels by the RR process, implying that these levels have long, but as yet undetermined, lifetimes. Such a phenomenon could form the basis of an infrared laser.

Finally, in this section, attention is drawn to recent work on the radical anions S$_2^-$ and Se$_2^-$ in ultramarines.[72] The ultramarine host lattice has a structure in which the radicals are trapped and stabilized in octahedral holes in the aluminosilicate lattice. Detailed measurements of the exci-
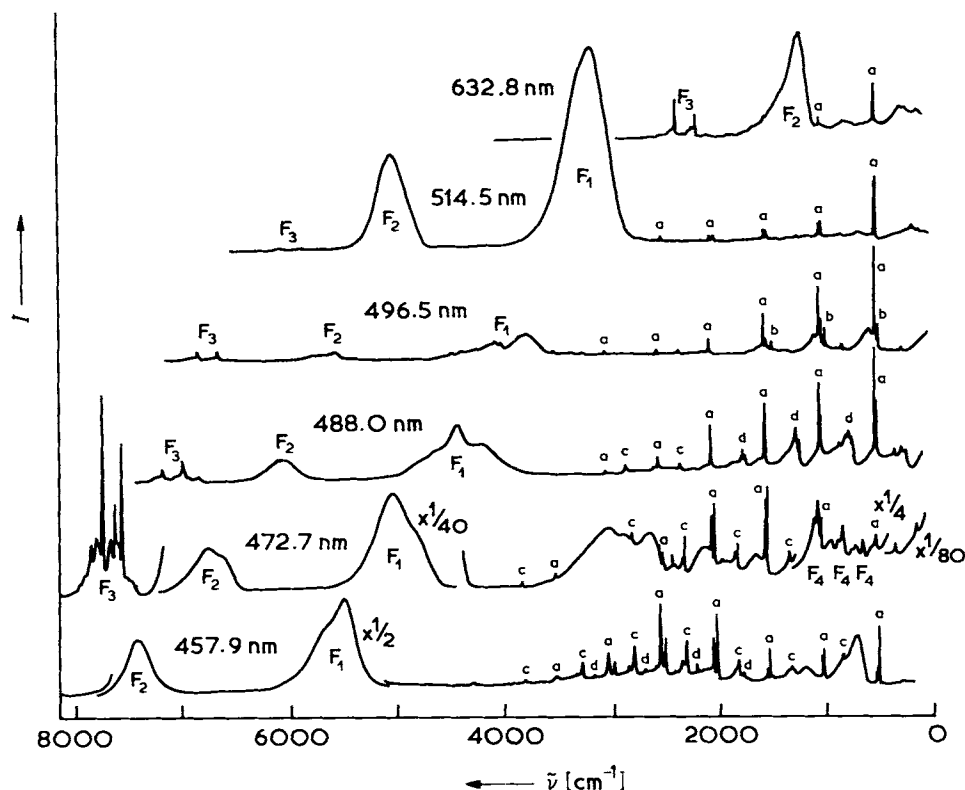
144

Angew. Chem. Int. Ed. Engl. 25 (1986) 131–158

Fig. 12. Resonance Raman spectra of vanadium isolated in a solid argon matrix at 15 K, obtained using various excitation lines. The progressions consist of (a) ground state Raman bands, (b) excited state Raman bands, and (c) and (d) electronic Raman bands. The bands designated F1, F2, F3, and F4 are assigned to fluorescence (after Ref. [75]).

tation profiles of the v, $2v$, and $3v$ RR bands of the radicals were fitted to Equation (21), thus enabling the determination of the bond length changes attendant upon excitation. These are substantial (0.30 and 0.32 Å for S_2^- and Se_2^- respectively), reflecting the decrease in bond order from 1.5 in the $^2\Pi_u$ ground state to 0.5 in the $^2\Pi_g$ excited state. The potential use of ultramarine host lattices for trapping other small species (both stable and unstable) offers an attractive possibility for their detailed investigation by RR spectroscopy.

4.2. Triatomic and Tetratomic Molecules

A summary of the recent investigation on the RR spectra of triatomic molecules is given in Table 3. Several of these have been concerned with the characterization of metal trimers in noble gas matrices. The properties of metal trimers are less well established than for dimers but structural information on the former is of importance since it is only with these that a proper comparison between cluster and bulk metal properties can be made. However, at this early stage there is still considerable controversy over electronic band assignments. Most of the spectra obtained can be interpreted in terms of a C_{2v} or distorted D_{3h} ground state for the scattering species but, in the case of Cu_3, evidence has been obtained to show that it is a Jahn-Teller fluxional molecule, pseudorotating even at 15 K.

RR data pertaining to tetratomic molecules are summarized in Table 4. Although there have been fewer studies of

tetratomic molecules than of diatomic and triatomic species, a number of important features of these studies are worthy of comment. The recently reported investigation of gaseous NH_3 heralds a new era of RR studies involving the use of far-UV excitation. By using the fifth harmonic of a pulsed Nd:YAG laser (212.8 nm), Ziegler and Hudson[96] were able to excite the singlet electronic transition of lowest energy (ca. 190 nm) assigned to the transfer of an electron from the nitrogen lone pair to a 3s Rydberg-type orbital. This excitation results in a change of molecular geometry from C_{3v} to D_{3h}, as evidenced by a long overtone progression in the deformation mode v_2 in the absorption spectrum. The RR spectrum displays a progression $v_2 v_2$ extending to $v_2 = 4$ and also a combination band progression $v_1 + v_2 v_2$ extending to $v_2 = 4$. This latter observation constitutes the first direct evidence from which it may be concluded that the N-H bond length changes upon excitation to the 190-nm state. Measurements of excitation profiles should enable the N-H bond-length change to be calculated.

The square planar molecules S_4^{2+}, Se_4^{2+}, and Te_4^{2+} are 6π-electron systems and they are thus examples of inorganic aromatic molecules. In each case the allowed electronic transition of lowest energy is $\pi^* \leftarrow \pi$ ($^1E_u \leftarrow ^1A_{1g}$), corresponding to the transfer of a electron from the nonbonding e_g orbital to the antibonding b_{2u} orbital. Excitation within the contour of the relevant absorption bands gives rise to RR spectra that are characterized by an intense progression $v_1 v_1$ and weaker subsidiary progressions

Angew. Chem. Int. Ed. Engl. 25 (1986) 131-158

145

Table 3. Resonance Raman data on triatomic species.

Species	State	Electronic band assignment	λ_{max} [nm]	λ_0 [nm]	ω_1 [cm⁻¹]	x_{11} [cm⁻¹]	Comments	Ref.
ClO_2	CFCl₃ soln., 295 K	$^2A_2 \leftarrow ^2B_1$	362	457.9	951.2	−4.8	$\omega_2=451.4$ cm⁻¹, $x_{12}=-8.1$ cm⁻¹; $\Delta Q_1=0.81$ Å amu$^{1/2}$ and $\Gamma=240$ cm⁻¹ [a]	[83, 84]
Cr_3	Ar matrix, 12-15 K			514.5	313	−2	$\nu_2=123$ cm⁻¹, $\nu_3=226$ cm⁻¹	[65]
Cu_3	Ar matrix,12-15 K			595.9	[b]	[b]	Pseudorotating JT molecule	[85]
I_3^-	Cs⁺ salt in Ar matrix, 12-16 K	$\sigma_u^* \leftarrow \pi_g$	355	476.5	113.4±0.2	−0.32±0.04		[86]
Ni_3	Ar matrix, 10 K			488.0	232.3	−1.0	Bond angle 90-100° [c]	[87]
NO_2	Ar, Kr and Xe matrices, 15 K	$^2B_2 \leftarrow ^2A_1$	≈500	488.0, 514.5	(Ar) 1326.5±0.5	−6.0±0.5	$x_{22}=-0.6\pm0.3$, $x_{13}=-29\pm3$, $x_{33}=-25\pm3$ cm⁻¹	[88]
					(Kr) 1329.1±0.5	−7.5±0.5	$x_{22}=-0.7\pm0.3$, $x_{13}=-31\pm3$, $x_{23}=-10\pm1$, $x_{33}=-25\pm2$ cm⁻¹	
					(Xe) 1321.9±0.5	−6.1±0.5	$x_{22}=-0.8\pm0.1$, $x_{13}=-31\pm3$, $x_{23}=-12\pm1$, $x_{33}=-30\pm3$ cm⁻¹	
O_3^-	γ-irradiated NaClO₃, 11 K	$^2A_2 \leftarrow ^2B_1$	≈440	457.9	(a) 1031.6 (b) 1034.5	−4.4 −3.25	$\Delta Q_1=0.63$ Å amu$^{1/2}$, $\Gamma=514$ cm⁻¹ [a, d]. (a), (b): non-equivalent sites of the O_3^- ions	[89]
	γ-irradiated Ba(ClO₃)₂·2H₂O			457.9	(a) 1050 (b) 1060	−11.2 −12.6		[90]
	γ-irradiated AgClO₃			514.5	(a) 1009 (b) 1023	−5.4 −8.4		[91]
	γ-irradiated Cd(ClO₃)₂, 15-300 K			457.9	1022	−3		[92]
Pb_3	Xe matrix, 12 K		455	488.0	117	−0.2	D₃ₕ geometry. $\nu_2(e')=96$ cm⁻¹	[68, 69]
S_3^-	DMF soln. HMPA soln. [f]	$^2A_2 \leftarrow ^2B_1$	600	647.1	537.5 536.1	−1.3 −1.3		[71]
Sb_3	Ar matrix, 13 K			476.5	~218	~0.3		[93]
Sc_3	Ar matrix, 12-15 K			676.4	247	−0.5	Geometry close to D₃ₕ, $\nu_2=145$ cm⁻¹, $\nu_3=151$ cm⁻¹. Electronic Raman transition at 395 cm⁻¹	[67]
$^{80}Se_3$	Ar and N₂ matrices, 15 K			514.5	312.15±0.2	−0.53±0.02		[94]
Te_3	N₂ matrix, 15 K			647.1	($^{126}Te_3$) 206.33±0.15 ($^{130}Te_3$) 203.1±0.1	0.24±0.03 0.22±0.05	C₂ᵥ geometry, $\theta=120\pm10°$ (from calculations). Multiple bonding inferred from $f_r+f_{rr}=2.1\pm0.1$ mdyn Å⁻¹	[95]

[a] From calculations of excitation profiles. [b] Irregular overtone progression precludes calculation. [c] Deduced from isotopic fine structure. [d] From calculations of the absorption spectrum. [e] Estimated from observation of overtone at 192 cm⁻¹. [f] HMPA = hexamethylphosphoric acid triamide.

Table 4. Resonance Raman data on tetratomic species.

Species	State	Electronic band assignment	λ_{max} [nm]	λ_0 [nm]	ω_1 [cm⁻¹]	x_{11} [cm⁻¹]	Comments	Ref.
Bi_4	Ar and Kr matrix, 8-10 K		670	676.4	152.5	−0.3		[60, 61]
NH_3	45 torr, 295 K	$^1A_2'' \leftarrow ^1A_1'$	192	212.8	[a]	[a]	Molecular geometry changes to D₃ₕ in the excited state as evidenced by RR activity of ν_2	[96]
S_4^{2+}	Soln. in 65% oleum	$^1E_u \leftarrow ^1A_{1g}$	330	350.7	584.7±0.5	−0.35±0.05	$x_{12}=-0.5\pm1$ cm⁻¹	[97]
Se_4^{2+}	Soln. in 25% oleum	$^1E_u \leftarrow ^1A_{1g}$	410	406.7	321.8±0.5	−0.55±0.05	$x_{12}=-1.3\pm1.0$ cm⁻¹	[97]
Te_4^{2+}	Soln. in conc. H₂SO₄	$^1E_u \leftarrow ^1A_{1g}$	510	514.5	219.5±0.5	−0.30±0.05		[97]
	Te₄[Al₂Cl₇]₂ solid, 80 K				214.1±0.5	−0.16±0.05	$x_{12}=-0.8\pm0.5$ cm⁻¹	
$[S_3N]^-$	[Ph₃P=N=PPh₃]⁺-salt, 295 K	$^1A' \leftarrow ^1A'$	468	488.0			Progressions observed involving all three stretching fundamentals, indicating that the electronic transition is delocalized over all four atoms	[92]

[a] Irregular overtone progressions precluded the calculation of molecular constants.

$v_1 v_1 + v_2$ and $v_1 v_1 + v_3$, the latter being evidence for excited-state JT effects involving $Q_2(b_{1g})$ and $Q_3(b_{2g})$. However, for Se_4^{2+} and Te_4^{2+}, v_3 is overlapped by v_1, as evidenced by $\rho(\pi/2) = 0.33$. For excitation resonant with an E_u state (x,y-polarization) the theoretical requirement is that $\rho(\pi/2) = 1/8$ for v_1 and $3/4$ for v_3; thus the measured ρ value for the overlapping bands results from an intensity ratio $I(v_1)/I(v_3)$ of 1.3. An analysis of the vibrational data showed that the coalescence of v_1 and v_3 arises because the interaction force constant associated with two adjacent bonds (f_{rr}) is near zero.

4.3. Tetrahedral Molecules

RR investigations of tetrahedral species (Table 5) have been centered on (a) transition metal oxo- and thio-anions, and (b) main group and transition metal tetrahalides. In each case excitation was into the contour of the charge-transfer absorption band of lowest energy in the visible/near UV region. The resonant electronic transition involves the promotion of an electron from the t_1 orbital localized on the ligands to the e metal-ligand antibonding orbital (Fig. 13). Such an electronic transition results in a significant lengthening of the bonds; thus the RR spectra are characterized by intense overtone progressions in the $v_1(a_1)$ mode. Additionally, subsidiary progressions are observed which involve single quanta of one or more of the non-totally symmetric modes $v_2(e)$, $v_3(t_2)$ and $v_4(t_2)$, i.e. progressions of the type $v_1 v_1 + v_2$, etc. These are attributed to JT coupling in the triply degenerate excited state, all three non-totally symmetric modes being potentially JT active.

In cases where the absorption spectra and excitation profiles display vibrational fine structure, serious attempts have been made to calculate the bond-length changes attendant upon excitation by fitting the experimental data to Equation (21). These bond-length changes, which range from 0.029 Å for $[WS_4]^{2-}$ to 0.046 Å for $[MnO_4]^-$, are
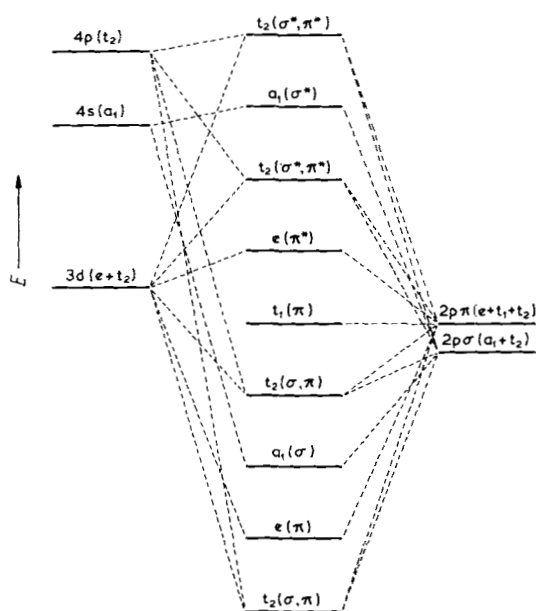
given in Table 4, together with the other parameters involved in the calculations. However, all of the bond-length changes determined for tetrahedral molecules have been miscalculated due to use of an erroneous relation between Δr and ΔQ. The values in the literature[24, 99, 102, 112, 115] are a factor of two greater than the correct ones, which are given in this review. The absorption spectrum and experimental and calculated EPs for $[MnO_4]^-$: $K[ClO_4]$ are shown in Figure 14. By comparison with the bond-length changes determined for the diatomic species (e.g. 0.30 Å for S_2^-), these values are small. This is because the change of bond order upon excitation is also much smaller, from 2.25 to 2.125, as compared to 1.5 to 0.5 for S_2^-.
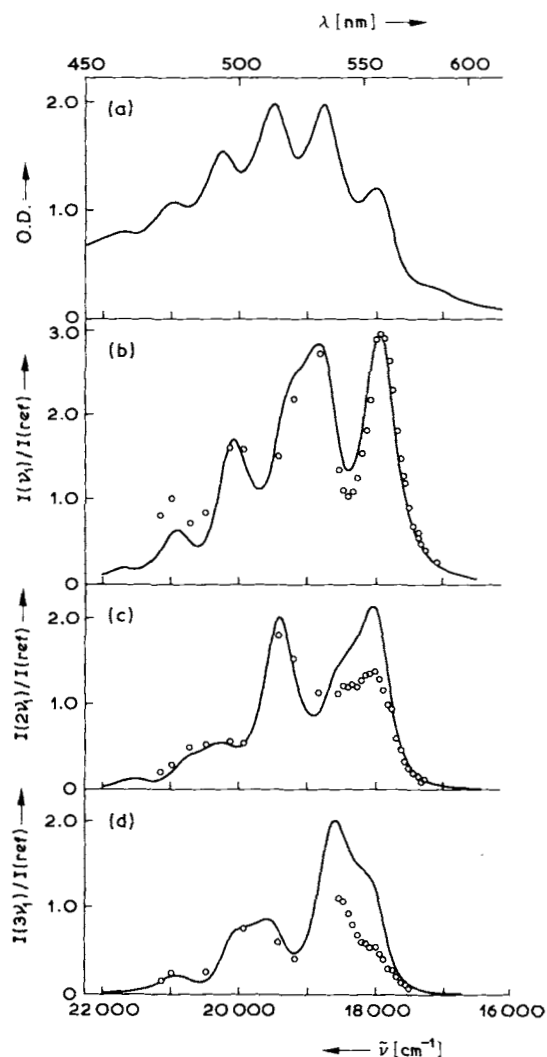

Fig. 14. (a) Absorption spectrum of $[MnO_4]^-$: $K[ClO_4]$ in a $K[ClO_4]$-disk at room temperature. O.D. = optical density. (b)–(d) Experimental (○) excitation profiles for the v_1, $2v_1$, and $3v_1$ bands of $[MnO_4]^-$, respectively. The full lines represent the (best fit) calculated profiles for $\Gamma = 300$ cm^{-1}, $\gamma = 0$, and $\Delta r = 0.46$ Å (after [24]).

Fig. 13. Schematic molecular orbital diagram for tetrahedral transition-metal complexes.

The electronic spectrum of $[WS_4]^{2-}$ in the 400–450 nm region consists of a strong band at ca. 400 nm and a weak shoulder at ca. 430 nm. The strong band has been assigned to the fully-allowed $^1T_2 \leftarrow ^1A_1$ transition arising from the $e \leftarrow t_1$ electronic transition. However, the excited $(t_1)^5(e)^1$ configuration gives rise to three other terms, $^1T_1$, $^3T_1$ and

147

Table 5. Resonance Raman data on tetrahedral XY$_4$ species.

Species	State	Electronic band assignment	λ_{max} [nm]	λ_0 [nm]	ω_1 [cm⁻¹]	x_{11} [cm⁻¹]	Comments	Ref.
$[CrO_4]^{2-}$	Ag$^+$ salt, Na$_2$SO$_4$ disk, 15 K	$^1T_2 \leftarrow {}^1A_1$		647.1			EP red-shifted from absorption maximum; no overtone progression observed	[98]
	aq. soln. 295 K			360–410			Measurement of v_1-EP; Calculations yielded $\Gamma = 730$ cm⁻¹, $\Delta r = 0.039$ Å, $\tilde{v}_{00} = 24\,987$ cm⁻¹	[99]
$[FeBr_4]^-$	[Bu$_4$N]$^+$ salt, KBr disk, 80 K	$^6T_2 \leftarrow {}^6A_1$	472	476.5	203.8 ± 0.2	−0.35 ± 0.05	$x_{13} \approx 1$ cm⁻¹	[52, 56, 100]
$[FeCl_4]^-$	[Et$_4$N]$^+$ salt, MeNO$_2$ soln., 295 K	$^6T_2 \leftarrow {}^6A_1$	365	363.8	335.2 ± 0.2	−0.54 ± 0.07		[52]
GeI$_4$	C$_6$H$_{12}$ soln., 295 K	$^1T_2 \leftarrow {}^1A_1$	360.4	363.8	158.9 ± 0.1	−0.09 ± 0.02		[101]
$[MnO_4]^-$	[MnO$_4$]$^-$:K[ClO$_4$], KBr disk, 295 K	$^1T_2 \leftarrow {}^1A_1$	545	514.5	848.6 ± 0.3	−0.88 ± 0.07	$x_{13} \approx -2.3$ cm⁻¹; $\Gamma = 300$ cm⁻¹ [a], $\Delta r = 0.046 \pm 0.003$ Å [a]	[24, 102, 103]
	[Ph$_4$P]$^+$ salt, KBr disk, 295 K			514.5	837.9 ± 0.4	−1.3 ± 0.2	$x_{13} \approx -2.6$ cm⁻¹; $\Gamma = 240$ cm⁻¹ [a], $\Delta r = 0.045$ Å [a]	[24, 103]
	^{18}O-enriched K[MnO$_4$], RbBr disk, 295 K			514.5	846.8 ± 0.1	−1.22 ± 0.09	[Mn^{16}O$_4$]$^-$	[104, 105]
					829.4 ± 0.1	−1.24 ± 0.09	[Mn^{16}O$_3{}^{18}$O]$^-$	
					817.8 ± 0.1	−1.18 ± 0.09	[Mn^{16}O$_2{}^{18}$O$_2$]$^-$	
					807.7 ± 0.1	−1.11 ± 0.09	[Mn^{16}O^{18}O$_3$]$^-$	
					798.4 ± 0.1	−0.99 ± 0.06	[Mn^{18}O$_4$]$^-$	
	[Ph$_4$As]$^+$ salt, 295 K			514.5	837.1 ± 0.5	−1.19 ± 0.1		[106]
	[Ph$_4$P]$^+$ salt, 295 K			514.5	836.4 ± 0.5	−1.04 ± 0.1		[106]
	[Et$_4$N]$^+$ salt, KBr disk, 80 K			514.5	838.9	−1.7		[107]
	Ag$^+$ salt, 295 K			514.5	797.0 ± 0.3	+1.4 ± 0.3	positive x_{11} value ascribed to polarizing effect of Ag$^+$ cation	[108]
$[MnO_4]^{2-}$	[MnO$_4$]$^{2-}$:CsI, 80 K	$^2T_2 \leftarrow {}^2E$	580	514.5	806.3 ± 0.4	−1.7 ± 0.1		[109]
	K$_2$[MnO$_4$], 295 K			514.5	818.3	−2.3		[104]
	Ba[MnO$_4$], 295 K			514.5	828.0	−3.3		[104]
	[MnO$_4$]$^{2-}$:K$_2$[CrO$_4$], 80 K			568.2	817.7 ± 0.5	−1.7 ± 0.2	$x_{13} = -2.0 \pm 0.5$ cm⁻¹; $\Gamma = 250 \pm 10$ cm⁻¹ [a], $\Delta r = 0.035 \pm 0.001$ Å [a], $\tilde{v}_{00} = 15\,900$ cm⁻¹ [a]	[110]
$[MoS_4]^{2-}$	aq. soln., 295 K	$^1T_2 \leftarrow {}^1A_1$	472	488.0	454	0 ± 0.5		[111]
	[Bu$_4$N]$^+$ salt, KBr disk, 80 K			476.5	452.0 ± 0.3	−0.47 ± 0.05	$x_{13} = -2.5 \pm 1.0$ cm⁻¹; $\Gamma = 265 \pm 10$ cm⁻¹ [a], $\Delta r = 0.035 \pm 0.003$ Å [a], $\tilde{v}_{00} = 20\,233$ cm⁻¹ [a]	[112]
$[MoSe_4]^{2-}$	aq. soln., 295 K	$^1T_2 \leftarrow {}^1A_1$	563	568.2	265	0 ± 0.5		[111]
$[PS_4]^{3-}$	Cu$^+$ salt, 80 K	$^1T_2 \leftarrow {}^1A_1$	480	476.5	393.3 ± 0.2	−0.46 ± 0.03		[113]
SnI$_4$	C$_6$H$_{12}$ soln., 295 K	$^1T_2 \leftarrow {}^1A_1$	364.5	363.8	151.2 ± 0.2	−0.02 ± 0.02		[101]
TiBr$_4$	C$_6$H$_{12}$ soln., 295 K	$^1T_2 \leftarrow {}^1A_1$	348.7	363.8	232.8 ± 0.1	−0.07 ± 0.01	$x_{12} = -0.8$, $x_{13} = -2.7$, $x_{14} \approx 0.7$ cm⁻¹	[114]
$[WS_4]^{2-}$	[NH$_4$]$^+$ salt, 80 K	$^1T_2 \leftarrow {}^1A_1$	395	406.7	490.5 ± 0.5	−1.1 ± 0.1		[115]
	[Bu$_4$N]$^+$ salt, 80 K				478.4 ± 0.5	−0.44 ± 0.05	$\Gamma = 100 \pm 10$ cm⁻¹ [a], $\gamma = 150 \pm 20$ cm⁻¹ [a], $\Delta r = 0.029 \pm 0.001$ [a], $\tilde{v}_{00} = 24\,650 \pm 10$ cm⁻¹ [a]	
$[WSe_4]^{2-}$	aq. soln., 295 K	$^1T_2 \leftarrow {}^1A_1$		488.0	279.5	0 ± 0.5		[111]

$^3T_2$, and the 430-nm shoulder has been assigned to the $^1T_1 \leftarrow {}^1A_1$ transition. The two other possible assignments are ruled out on the grounds that (a) the $^3T_2 \leftarrow {}^1A_1$ transition would be expected to be of much lower energy than $^1T_2 \leftarrow {}^1A_1$,[159] and (b) $^3T_1 \leftarrow {}^1A_1$ is both spin- and orbitally-forbidden. Excitation profiles measured throughout the $^1T_2 \leftarrow {}^1A_1$ and $^1T_1 \leftarrow {}^1A_1$ bands display minima in the region of the latter (Fig. 15). This behavior can be accounted for by interference between the $^1T_2$ and $^1T_1$ contributions to the transition polarizability. Calculations were performed on the assumption that Δr is the same for both states (Fig. 16). This seems reasonable as these two terms arise from
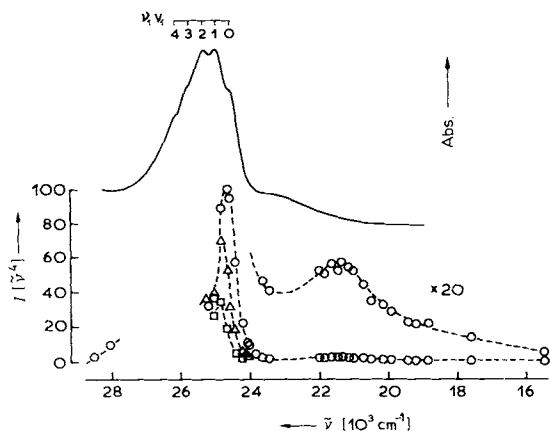
148

Fig. 15. Electronic absorption spectrum of [Bu₄N]₂[WS₄] at 14 K (solid line) and the excitation profiles for v_1 (o), $2v_1$ (Δ) and $3v_1$ (□) at 80 K (after Ref. [115]).

the same excited configuration. Corroborative evidence for the $^1T_1 \leftarrow {}^1A_1$ assignment is provided by the observation of, and analogous assignment for, similar bands in the absorption spectra of $[CrO_4]^{2-}$ [116] and $[MnO_4]^-$.[117] Unfortunately, these occur in less accessible regions (385 and 850 nm, respectively) and thus have not yet been subjected to RR investigation.
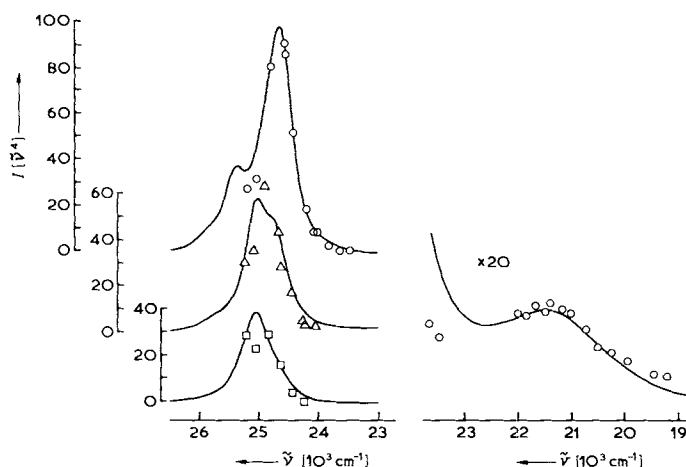
Fig. 16. Calculated (solid lines) and experimental excitation profiles for the v_1 (o), $2v_1$ (Δ), and $3v_1$ (□) bands of [Bu₄N]₂[WS₄] at 80 K (after Ref. [115]).

Attention is drawn to the observation of $\rho(\pi/2) = 0.15$ for the v_1 band of $[FeBr_4]^-$, where a value of zero might, at first sight, be expected. The non-zero value has been shown to be due to an antisymmetric contribution to the transition polarizability tensor,[56, 100] resulting from spin-orbit coupling of the $^6A_1$ ground state with various excited states of the same spin multiplicity. The magnitude of the antisymmetric tensor contribution is likely to be governed by the spin-orbit coupling constant for both the metal and ligand atoms, and the reciprocal of the energy separation between the ground state and those excited states to which it is coupled. On this basis it would be expected that v_1 $\rho(\pi/2)$ values for the series of molecules $[FeX_4]^-$ would increase in the order X = Cl < Br < I. Partial support for

this hypothesis is provided by the observation that $\rho(\pi/2) = 0$ for the v_1 band of $[FeCl_4]^-$. Studies on the $[FeI_4]^-$ molecule were precluded by its rapid decomposition in solution.

4.4. Planar Four-Coordinate Molecules

There have been no new reported RR studies on square planar MX₄-type molecules during the last few years, and the reader is referred to earlier reviews[1, 23] for examples of these. However, there have been a number of RR investigations of bis(dithio) complexes of nickel(II)[118-123] and copper(II),[120, 121] which have assisted in the electronic band assignments for these molecules. The copper complexes are of particular interest as they are model compounds for the study of copper(II)-sulfur interactions in blue copper proteins. In all of the systems studied, absorption bands in the visible region were assigned to metal-ligand charge transfer (MLCT) transitions on the basis that excitation within the contours of these bands yields intense RR spectra dominated by several totally symmetric modes. Due to the lack of bands attributable to either overtones or non-totally symmetric modes in most of these spectra, it may be concluded that any changes of geometry in the MLCT excited states are confined to minor alterations of some bond lengths and angles. One notable exception is the "red" form of bis(dithiooxalato)nickel(II)[123] for which the following progressions were observed: $v_1 v_1$ extending to $v_1 = 6$, and $v_1 v_1 + v_2$ extending to $v_1 = 4$, where v_1 is a combination of CC and CS stretching coordinates and v_2 is a combination of CO and CC stretching coordinates. Clearly, there is a significant change in the size of the C_2S_2Ni ring upon electronic excitation.

4.5. Five-Coordinate Molecules

The only five-coordinate molecules to have been studied recently are the tetrahalooxotechnetate(V) ions, $[TcOX_4]^-$, where $X = Br$[124] or I.[125] For the bromide a progression reaching to $4v_4$ was observed, where v_4 is the b_1 class $v(TeBr_4)$ mode. This is clear evidence for a strong excited-state JT effect involving Q_4. Additionally, weak bands assigned to $2v_1$ and $2v_1 \pm v_4$ were observed, where v_1 is the $v(TcO)$ mode. The RR spectrum of the iodide displays a progression in $v_1 v_1$ extending to $5v_1$ ($\omega_1 = 1005.3 \pm 0.2$, $x_{11} = -4.7 \pm 0.1$ cm^{-1}) and several weaker progressions of the sort $v_1 v_1 + v_i$, where v_i is v_2, v_3, v_4, v_6 or an unidentified lattice mode. Weak first overtones of $v_2(a_1)$, $v_3(a_1)$, $v_4(b_1)$, and $v_8(e)$ are also observed and it may be concluded that excited-state JT effects are weaker for the iodide than for the bromide.

4.6. Octahedral Molecules

The results of RR studies of hexahalometalate ions are summarized in Table 6. The ions concerned are derivatives of d³, d⁴, and d⁵ transition metals and the $d^{10}s^2$ complexes $[TeX_6]^{2-}$, X = Br or Cl. The low spin d⁴ and d⁵ species are of special interest in that the $^3T_{1g}$ and $^2T_{2g}$ ground terms are split by spin-orbit interaction to give, respectively, four

Angew. Chem. Int. Ed. Engl. 25 (1986) 131–158

149

Table 6. Resonance Raman data on hexahalometalate ions. ER Bands = Electronic Raman bands. MROA-experiment = Magnetic Raman Optical activity experiment.

Species	State	Electronic band assignment	λ_{max} [nm]	λ_0 [nm]	ω_1 [cm^{-1}]	x_{11} [cm^{-1}]	Comments	Ref.
$[IrBr_6]^{2-}$	K$^+$ salt, aq. soln.	$U_u''(^2T_{2u}) \leftarrow E_g''(^2T_{2g})$ 604		510–680			[a]	[50]
	[Bu$_4$N]$^+$ salt, KBr disk, 80 K and 15 K			600	210.3	0±0.5	ER-band $\Gamma_8 \leftarrow \Gamma_7'(^2T_{2g})$ origin at 4990 cm^{-1}, progressions involving v_1 and v_5	[126, 127]
	K$^+$ salt, aq. soln.			514.5, 577.5			MROA-experiment; negative g-value for ground state	[128]
$[IrCl_6]^{2-}$	[Bu$_4$N]$^+$ salt, 15, 80 K	$U_u''(^2T_{2u}) \leftarrow E_g''(^2T_{2g})$ 495		488.0	341.4	0±0.3	ER-band $\Gamma_8 \leftarrow \Gamma_7(^2T_{2g})$ with origin at 5500 cm^{-1}, progressions involving v_1, v_2 and v_5	[126, 127, 129, 130]
	[Bu$_4$N]$^+$ salt, MeCN-soln., K$^+$ salt, HCl soln., 295 K						MROA-experiments have established a negative value for $E''(^2T_{2g})$ and positive one for $U'(^2T_{2g})$ [a]	[50, 131, 132]
$[OsBr_6]^{2-}$	[Bu$_4$N]$^+$ salt, 80 K	$2T_{1u} \leftarrow A_{1g}$	450	457.9	211.4	0±0.4	$x_{12} = -2±1$, $x_{15} = -0.5±1$ cm^{-1}; ER-bands at 2810, 4850, 5000 cm^{-1} assigned to $\Gamma_4 \leftarrow \Gamma_1$, $\Gamma_5 \leftarrow \Gamma_1$, $\Gamma_3 \leftarrow \Gamma_1$	[126, 133, 134]
	K$^+$ salt, HBr soln., 295 K			488.0			Assigments confirmed by ρ measurements, positive g factor for $\Gamma_4(^3T_{1g})$	[132, 134]
$[OsCl_6]^-$	[Et$_4$N]$^+$ salt, 80 K	$^4T_{2u} \leftarrow ^4A_{2g}$	500	488.0	376.6±0.6	−0.8±0.2	Band origin at 5800 cm^{-1} assigned to $\Gamma_8(^2T_{2g}) \leftarrow \Gamma_8(^4A_{2g})$. $\rho(\pi/2) = 0.2$	[135]
$[OsCl_6]^{2-}$	K$^+$ salt, HCl soln., 295 K	$T_{1u} \leftarrow A_{1g}$	324, 375	325, 454.5			ER-Bands at 2780, 5060 and 5190 cm^{-1} assigned to $\Gamma_4 \leftarrow \Gamma_1$, $\Gamma_5 \leftarrow \Gamma_1$ and $\Gamma_3 \leftarrow \Gamma_1$ on the basis of ρ measurements	[50, 134]
	[Bu$_4$N]$^+$ salt, 80 K			514.5			Electronic origins at 2800, 4880 and 5090 cm^{-1}	[127]
$[OsI_6]^{2-}$	K$^+$ salt, H[ClO$_4$] soln., 295 K	$T_{1u} \leftarrow A_{1g}$	387, 556, 565, 576	514.5			ER-bands at 2640, 4600 cm^{-1} (assigned to $\Gamma_4 \leftarrow \Gamma_1$ and $\Gamma_{3,5} \leftarrow \Gamma_1$ on the basis of ρ measurements)	[134]
	[Bu$_4$N]$^+$ salt, 80 K			647.1	156.9±1	−0.8±0.5	Band origins at 2580 ($\Gamma_4 \leftarrow \Gamma_1$), 4440 ($\Gamma_3 \leftarrow \Gamma_1$), 4710 cm^{-1} ($\Gamma_5 \leftarrow \Gamma_1$)	[127]
$[RuBr_6]^{2-}$	[Bu$_4$N]$^+$ salt, KBr disk, 80 K	$T_{1u} \leftarrow A_{1g}$ $(t_{2u}(\pi) \rightarrow t_{2g})$	580	568.2	200.8	−0.15	Band origins at 752 ($\Gamma_4 \leftarrow \Gamma_1$), 1850 cm^{-1} ($\Gamma_{3,5} \leftarrow \Gamma_1$)	[136]
$[RuCl_6]^{2-}$	[Ph$_4$P]$^+$ salt, KCl disk, 80 K	$T_{1u} \leftarrow A_{1g}$ $(t_{1u}(\pi,\sigma) \rightarrow t_{2g})$	520	501.7	326.5	−0.11	Band origins at 1529 cm^{-1} assigned to $\Gamma_{3,5} \leftarrow \Gamma_1$. Progression in $v_1 v_1$ based on this origin observed for $\lambda_0 = 457.9$ nm	[136]
$[TeX_6]^{2-}$ X = Br or Cl	[Bu$_4$N]$^+$ salts, MeCN solns., 295 K	$^{1,3}T_{1u} \leftarrow ^1A_{1g}$	320–470(Br) 260–405(Cl)	356.4 337.5			$\rho(\pi/2) = 0.18±0.02$ for $2v_2$ of $[TeBr_6]^{2-}$ in good agreeement with theoretical prediction (3/14)	[137]

[a] Anomalous depolarization ratios for v_1, v_2 and v_5 ascribed to antisymmetric tensor contributions resulting from ground-state degeneracy.

and two states (Fig. 17). These states all lie within ca. 5000 cm^{-1} of each other and in each case Raman bands have been observed which may be assigned to transitions from
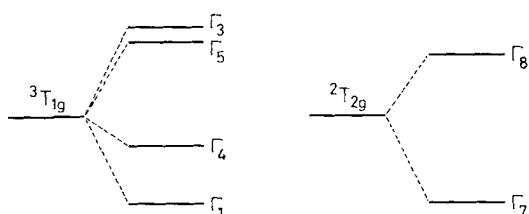

Fig. 17. Qualitative energy level diagrams for the spin-orbit splitting of the $^3T_{1g}$ and $^2T_{2g}$ ground terms.

the ground to these states. The most recently reported study is of the vibrational and electronic RR spectra of the $[RuCl_6]^{2-}$ and $[RuBr_6]^{2-}$ ions. The RR spectra and EPs for $[RuCl_6]^{2-}$ are shown in Figure 18. The electronic and vibrational Raman bands display maximum intensity for resonance with different excited states, although it is not understood why this should be so.

The 5d^5 species $[IrCl_6]^{2-}$ and $[IrBr_6]^{2-}$ possess Kramers degenerate $\Gamma_6(^2T_{2g})$ ground states. As a consequence of the ground-state degeneracy, the three Raman-active fundamentals (v_1, v_2 and v_5) all give rise to anomalously polarized bands.[50] Some of the hexahalometalates have been investigated by the relatively new technique of magnetic Raman optical activity, which enables the sign of the
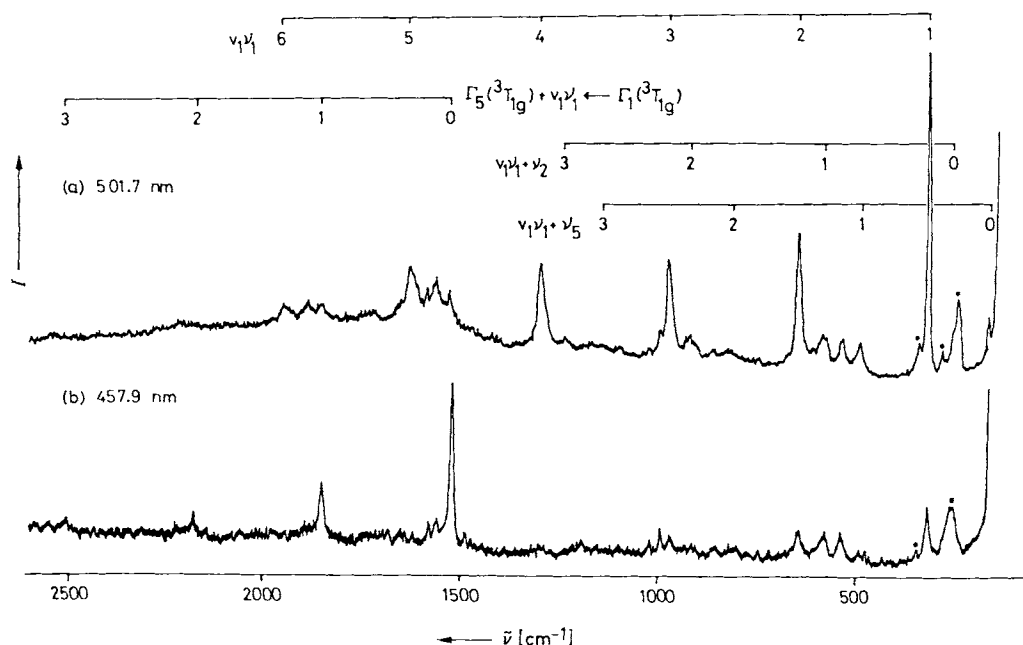
Fig. 18. Resonance Raman spectra of $[Ph_4P]_2[RuCl_6]$ in a CsCl disk at ca. 80 K excited by (a) 501.7 nm and (b) 457.9 nm radiation. Bands marked by an asterisk are due to impurities (after Ref. [136]).

ground-state g-factor to be determined from circular intensity differential measurements.[131]

4.7. Species with No Discrete Vibrating Unit

In this section we discuss some recent RR studies on the two-dimensional layer compounds ZrS_3[138] and HfS_3.[139] Although these are strictly semiconductor species we have chosen to include them because their RR behavior is in many ways similar to that of small molecular species. ZrS_3 has a band gap energy of about 2.5 eV (20000 cm^{-1}) and excitation in this region produces RR spectra that are dominated by progressions involving three fundamentals, at 152, 285, and 326 cm^{-1}. These are assigned to the vibrational R_y' motion, the totally symmetric stretching mode of Zr–S$_1$ interchain bonds, and the $v_s(ZrS_2^{2-})$ vibration, respectively. Off-resonance polarized Raman spectra indicate that the intensities of all three of these bands are dominated by α_{yy} components. Since the excitation profiles of these bands were found to maximize close to the absorption maximum at 492 nm, it was concluded that the transition must be y-polarized ($A_u \leftarrow A_g$ in the C_{2h} factor group). Neglecting any changes of vibrational wave number in the excited state, the best fit to the excitation profiles was calculated with the parameters $\bar{v}_{00} = 20325$ cm^{-1}, $\Gamma = 450$ cm^{-1}, and $\Delta = 0.894$ (285 and 326 cm^{-1} bands) or 1.0 (152 cm^{-1} band).

For HfS_3 the first absorption maximum is at ca. 22700 cm^{-1} and excitation in this region produces RR spectra and excitation profiles that are similar to those of ZrS_3. The most enhanced bands are the four totally symmetric modes at 128, 261, 275, and 322 cm^{-1}, which were shown by off-resonance Raman orientation measurements to be dominated by their α_{yy} components. It was postulated that at least two allowed y-polarized transitions contribute to the RR scattering process for both HfS_3 and ZrS_3.

5. Resonance Raman Studies of Larger Polyatomic Molecules

5.1. Six-Coordinate Transition Metal Complexes

There have been a number of RR studies of tris(α-diimine) and related complexes of iron(II),[140–145] ruthenium(II),[146–152] and, to a lesser extent, osmium(II).[141,148] A great deal of interest has been focused on $[Ru(bpy)_3]^{2+}$, bpy = 2,2'-bipyridyl, because of its importance as a photocatalyst for the photodecomposition of water. RR investigations of $[Ru(bpy)_3]^{2+}$ have involved (a) excitation resonant with the first singlet MLCT excited state at 22000 cm^{-1}, and (b) optical pumping of the first triplet MLCT state (via the singlet), designated $[*Ru(bpy)_3]^{2+}$, followed by resonant excitation from the populated triplet state to a higher triplet state. The latter enables the measurement of the RR spectrum of the ion in the first triplet excited state. This is characterized by a number of new vibrational bands which are ca. 60 cm^{-1} lower than for the ion in its ground state. The similarity between these bands and those of the bipyridyl radical anion have led to the conclusion that the electron transfer from the metal is to one bpy ligand only (rather than to a molecular orbital encompassing all three), such that the excited state may be formulated as $[Ru^{III}(bpy)_2(bpy^{\bullet -})]^{2+}$. Additional evidence for the localized model is provided by (a) the observation of additional bands which are unshifted with respect to the ground state, indicating the presence of neutral bipyridyl ligands in the excited state, (b) similar behavior for $[Os(bpy)_3]^{2+}$, substituted bis(bipyridyl)ruthenium(II) complexes, and fac-$[XRe(CO)_3(bpy)]$, X = Br or Cl.[148,152]

Tris(α-diimine)iron(II) complexes exhibit a strong absorption band in the visible region ($\lambda_{max} = 524$ nm for $[Fe(bpy)_3]^{2+}$) which has been assigned to a MLCT $^1E \leftarrow {}^1A_1$ transition on the basis of single-crystal polarized absorp-

tion studies. In each case there is an unresolved shoulder ca. 1500 cm^{-1} above the absorption maximum, which could be assigned to a vibronic side-band or to a second electronic transition. RR spectra and excitation profiles of these complexes have been measured using excitation throughout the absorption region and the results interpreted in terms of a single transition giving rise to a 0-0 and a conglomerate of 0-1 bands.[140] This conclusion was reached on the bases that (a) the most enhanced Raman bands are those in the 1400-1600 cm^{-1} region (ligand ring vibrations involving C–C and C–N bonds) and (b) these modes are responsible for the vibronic sideband in the absorption spectra. However, the RR band depolarization ratios vary between 0.10 and 0.71,[140] an observation which is inconsistent with RR scattering involving only a $^1E \leftarrow ^1A_1$ resonant transition $(\rho(\pi/2) = 1/8$ for totally symmetric modes), but which could be accounted for by contributions from both ^1E and $^1A_2$ resonant excited states. New absorption and CD spectroscopic data obtained for [Fe(bpy)$_3$]$^{2+}$ indicate that there may be a number of transitions within this spectral region.[153] A reassessment of the RR spectrum of the ion is in progress in our laboratory.

A number of carbonyl-imine and -diimine complexes of Cr, Mo, W, Re and Fe have been investigated by *Stufkens* et al.[154-157] The RR spectra of these complexes were obtained by excitation within the MLCT band of lowest energy, i.e. in the 400-600 nm region. In common with the diimine complexes discussed previously, the spectra display only polarized Raman bands. Thus the scattering mechanism is undoubtedly of A-term origin and the small displacement approximation is probably valid because any bands attributable to overtones are very weak. The MLCT bands have been shown to consist of the overlap of three or four bands on the basis of RR EPs and magnetic circular dichroism spectra. These bands are assigned to charge transfer resulting from the promotion of an electron from one of the metal d-orbitals to a π^* orbital localized on the diimine ligand. The RR data are consistent with this assignment in that the most enhanced Raman bands are those associated with the diimine ligand, i.e. bands in the 1400-1600 cm^{-1} region which are attributed to ν(CC) and ν(CN) stretching modes. Surprisingly, it is found that the ν_s(cis-CO) bands are also enhanced, which implies that the CO bond lengths are affected by transitions to an MLCT state. That the ν_s(trans-CO) bands do not display RR activity suggests that the effect is not due either to the oxidation of the metal atom or to a change of π-backbonding accompanying the transition. Instead, it is believed that the RR activity of ν_s(cis-CO) is due to an excited state interaction between the diimine and the cis-carbonyl ligands. Such an interaction is expected to increase as the central atom becomes smaller, this inference being supported by the observation that, for the series [M(CO)$_4$(diazabutadiene)], where M = Cr, Mo, or W, the intensity of ν_s(cis-CO) increases with respect to ν_s(CN) in the order W < Mo < Cr. It was also found that these compounds are photoreactive when irradiated in the presence of a phosphane ligand within the MLCT band. This process results in the substitution of a cis-carbonyl group by the phosphane with a quantum yield varying from 10^{-2} to 10^{-4}. The quantum yield is found experimentally to be directly related to the

Raman intensity of the ν(cis-CO) band, and complexes which do not display a RR effect for this vibration are photochemically stable. These results clearly show that RR spectroscopy is a powerful tool for the interpretation of the photochemistry of inorganic molecules.

RR studies of K$_3$[Cr(CN)$_5$NO][158] at resonance with the $^2B_2 \leftarrow ^2B_1$ chromium-to-NO transition have shown that the most enhanced Raman band, and the one which forms the longest (to three members) progression, is ν(CrN). Intensity ratio calculations have led to the conclusion that the CrN bond length increases by ca. 0.10 Å on excitation to this MLCT state, but that the CrC bond length also increases, though by a lesser amount (ca. 0.07 Å).

5.2. Metal–Metal Bonded and Bridged Species

Of the very large number of metal-metal bonded species known,[160] those for which RR studies have proved to be particularly valuable are the quadruply bonded ones [Mo$_2$Cl$_8$]$^{4-}$, [Mo$_2$Br$_8$]$^{4-}$, and [Re$_2$X$_8$]$^{2-}$, X = F, Cl, Br, or I.[161-166] In each case the eight halogen atoms are situated virtually at the corners of a cube, thereby encapsulating the M$_2$ unit, the MMX angle being ca. 105° in each case. The molybdenum and rhenium species are effectively isoelectronic, the molybdenum species possessing a single moderately intense and highly structured band in the visible region. The principal progression-forming mode giving rise to this structure has, in each case, been identified as the MM stretch. For the rhenium species there are a number of bands throughout the visible/near UV region (Fig. 19). The lowest energy band in each case, as for the molybdenum
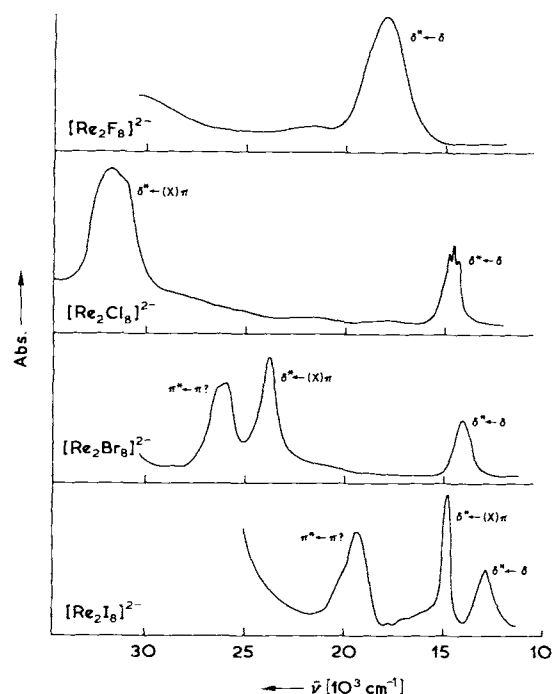

Fig. 19. Electronic absorption spectra of the complexes [Bu$_4$N]$_2$[Re$_2$X$_8$] at ca. 14 K in the region of their $\delta^* \leftarrow \delta$, $\delta^* \leftarrow \pi$(X) and $\pi^* \leftarrow \pi$ (?) transitions. (Cs[BF$_4$], KCl, KBr, and CsI disks for X = F, Cl, Br, or I, respectively) (after Ref. [167]).

species, has been assigned to the $^1A_{2u} \leftarrow {}^1A_{1g}$ ($\delta^*(b_{1u}) \leftarrow \delta(b_{2g})$) transition. Excitation of such an ion from the ground to the $^1A_{2u}$ state in effect changes the MM bond order from four to three, with consequential increase in bond length (hence the observed progression in $\nu(MM)$).

Irradiation within the contour of the $\delta^* \leftarrow \delta$ band leads, in each case, to the generation of an RR spectrum characterized by (a) substantial enhancement to the intensity of $\nu(MM)$ and (b) the development of a long (at most to eleven members) progression in $\nu(MM)$. These results confirm the conclusion drawn from the electronic spectra, namely that the equilibrium MM bond length in the δ^* state is significantly longer than that in the ground state. The set of four dirhenium anions are particularly interesting (Fig. 20). Raman spectra of these ions, in each case obtained at resonance with the $\delta^* \leftarrow \delta$ transition, give rise to long progressions in $\nu(ReRe)$ (318, 275, 276, and 257 cm^{-1} for X = F, Cl, Br, or I, respectively); these observations clearly indicate the similar nature of the lowest electronic transition in each case. This conclusion is substantiated by measurements of the depolarization ratio of the $\nu(ReRe)$ Raman band at resonance with the $\delta^* \leftarrow \delta$ transition. This has been found to take the value 1/3 for $[Re_2F_8]^{2-}$, $[Re_2Cl_8]^{2-}$ and $[Re_2Br_8]^{2-}$, a result which is only possible if the resonant electronic transition is z-polarized (Section 2.5). This is precisely the polarization of the $\delta^* \leftarrow \delta$ transition (transition moment A_{2u} in the D_{4h} symmetry point group to which the ions belong).[167, 168]
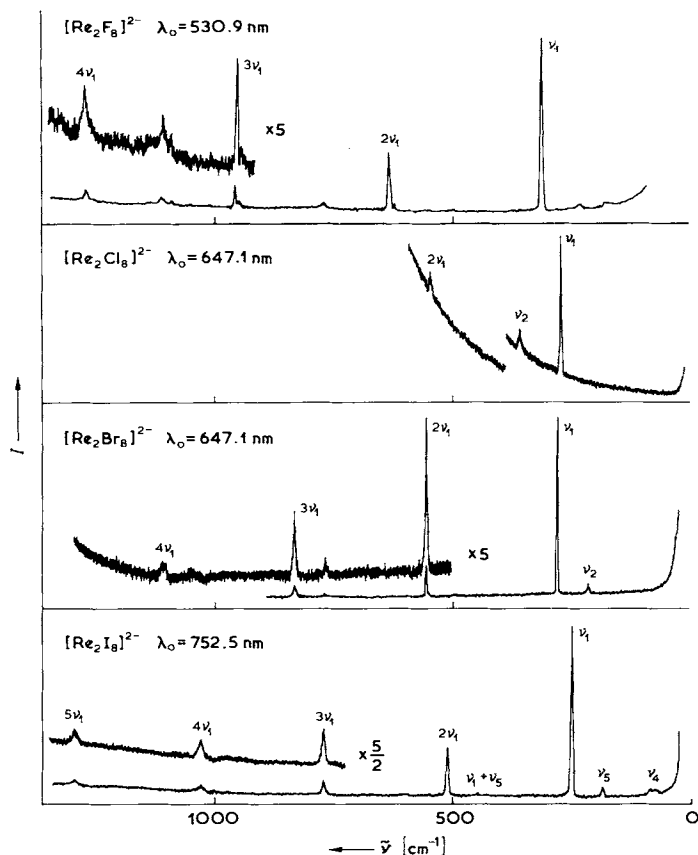
Fig. 20. Resonance Raman spectra of the complexes $[Bu_4N]_2[Re_2X_8]$ at ca. 80 K in the region of their $\delta^* \leftarrow \delta$ transitions (after Refs. [167], [168]).

Irradiation within the contour of the second electronic transition of each ion produces substantially different spectra in each case (Fig. 21). Such RR spectra are characterized by resonance enhancement to the bands attributed to $\nu(ReX)$ and its overtones. ($\nu(ReX)$ occurs at 624, 362,
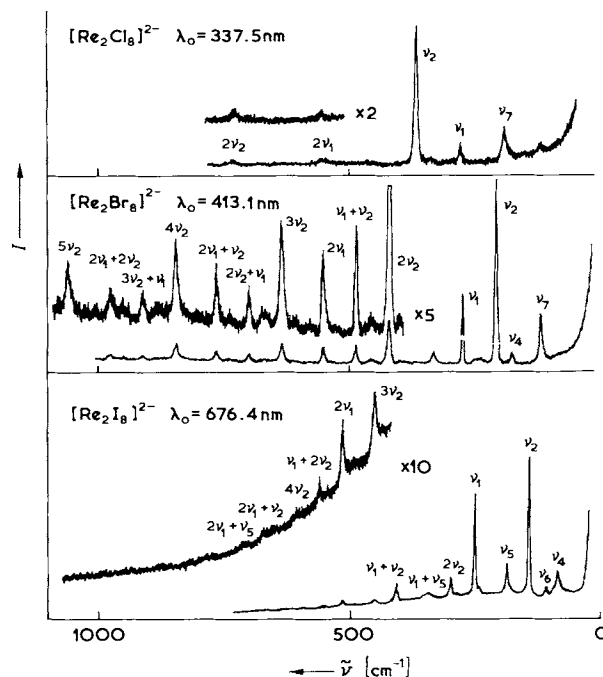
Fig. 21. Resonance Raman spectra of the complexes $[Bu_4N]_2[Re_2X_8]$ at ca. 80 K in the region of their $\delta^* \leftarrow \pi(X)$ transitions (after Refs. [167], [168]).

211 and 152 cm^{-1} for X = F, Cl, Br or I, respectively). Thus, the principal structural change undergone by each ion on excitation to its second excited state is along the ReX coordinate. This result clearly implies that the second electronic transition is in each case of the halogen-to-metal charge-transfer type. The assignment of the second strong band in the electronic spectra of the $[Re_2X_8]^{2-}$ ions is thus clearly $b_{1u}(\delta^*) \leftarrow X, e_g(\pi)$, $^1E_u \leftarrow {}^1A_{1g}$. This result is confirmed by the fact that the measured depolarization ratio of the $\nu(ReX)$ band of $[Re_2Cl_8]^{2-}$ and $[Re_2Br_8]^{2-}$ at resonance with the second electronic band is 0.15, i.e. close to the value of 1/8, as required for a $^1E_u \leftarrow {}^1A_{1g}$ transition.

Many other metal-metal multiply bonded species yield richly detailed RR spectra at resonance with their lowest electronic transition. The most notable of the recent studies along these lines have been those on $[Ru_2(O_2CR)_4Cl]$, R = H, CH$_3$, C$_2$H$_5$, or C$_3$H$_7$,[169] and related studies on diosmium and dirhodium carboxylates.[170, 171] In addition to the bond between them the metal atoms are bridged by the carboxylate ligands.

Another type of bridged species is that in which the metal atoms are separated by one or more atoms. Of these, $[Ru_2OCl_{10}]^{4-}$ (Fig. 22) and related ions have been subjected to the most intensive RR investigations.[172, 173] The spectra of these ions are characterized by intense progressions involving the M–O–M stretching coordinate (ν_1), the axial and equatorial metal–halogen stretches (ν_2 and ν_3), the $\delta(OMX_{eq})$ coordinate (ν_4), and even quanta of the infrared-active modes $\nu_5(\nu_{as}(MOM))$ and $\nu_9(\delta(MOM))$. It is

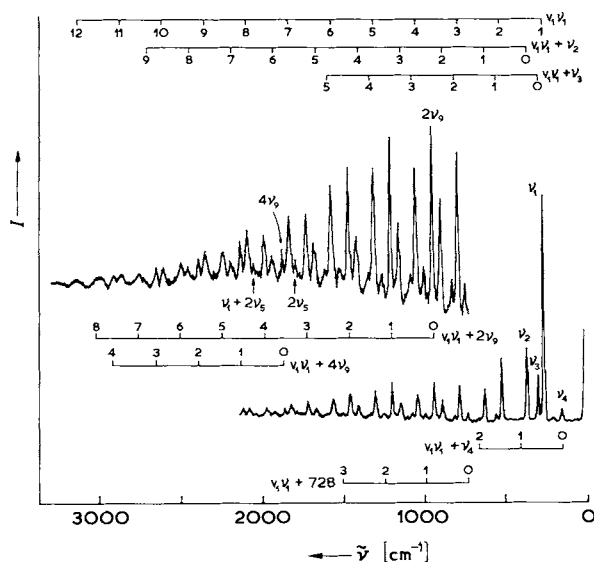*Angew. Chem. Int. Ed. Engl. 25 (1986) 131–158*

153

Fig. 22. Resonance Raman spectrum of $K_4[Ru_2OCl_{10}]$ at ca. 80 K, obtained with 488.0 nm excitation (after Ref. [173]).

clear, then, that there must be a substantial alteration of molecular geometry accompanying the resonant, $^1A_{2u} \leftarrow {}^1A_{1g}$, electronic transition. The observation of progressions involving even quanta of $v_5(a_{2u})$ and $v_9(e_u)$ is strong evidence for a reduction in symmetry in the excited state, although it is not obvious what that symmetry might be.

Other bridged species that have been studied recently include ones in which the bridging moiety is $N,^{[174]}$ $N_2,^{[175]}$ or O_2 (both peroxo and superoxo).[176] In all cases the RR spectra are characterized by a number of bands attributable to totally symmetric fundamentals. Together with the absence of any overtones for most of these species this observation indicates that the geometric changes attendant upon excitation are small and spread over many atoms.[38] There have been several studies of μ_2- and μ_3-sulfur-bridged species in which there are $[MS_4]^{2-}$ sub-units, where $M = Mo$ or $W.^{[177-179]}$ Considerable interest has developed in the molybdenum complexes, some of which are model compounds for the MoFe cofactor of nitrogenase.

5.3. Mixed-Valence Complexes

Complexes in which the metal atom is present in more than one oxidation state are of considerable importance, not only in inorganic chemistry, but also in bioinorganic chemistry and geology. Thus, at least 40 elements in the periodic table form mixed-valence complexes, many of which have very striking properties. Mixed-valency is central to the role of Fe_4S_4 clusters for promoting redox processes in enzymes such as ferredoxin and rubredoxin, and many minerals (particularly iron minerals) contain the metal in at least two oxidation states.

The two most significant properties of mixed-valence complexes are their colors and their electrical conductivities. Each of these properties differs substantially, in many cases, from those of the constituent single-valence species. In the first place, the colors of certain mixed-valence spe-

cies are so intense that they have been used as dyestuffs (e.g. Prussian blue, ruthenium red), while in the second place, certain mixed-valence complexes are best described as one-dimensional conductors (e.g. $[K_2Pt(CN)_4 \cdot Br_{0.30} \cdot 3 H_2O]$ (KCP)). The reader is referred elsewhere to recent reviews of the classification and properties of mixed-valence complexes.[3,4]

The colors of mixed-valence complexes are dominated by intervalence transitions which, being electric-dipole allowed, are in general intense. Raman studies of such complexes at resonance with the intervalence bands prove to be very sensitive probes of the geometric changes undergone on excitation from the ground to the intervalence state. Particularly detailed studies of certain types of linear-chain complexes have now been made, viz. that of Wolffram's red and its analogues, which are examples of Pt^{II}/Pt^{IV} mixed-valence complexes of the type 1, where

1
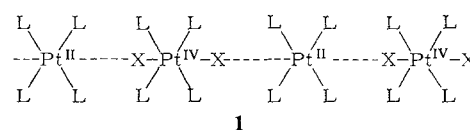
$L = $ amine, $X = Cl$, Br, or I. Irradiation within the contour of the intervalence band of such complexes leads to enormous intensification of the band attributed to the symmetric chain-stretching mode, $v_1(X-Pt^{IV}-X)$, together with the development of a long, intense, overtone progression $v_1 v_1$ (reaching to, at most, 18 members) (Fig. 23). These results
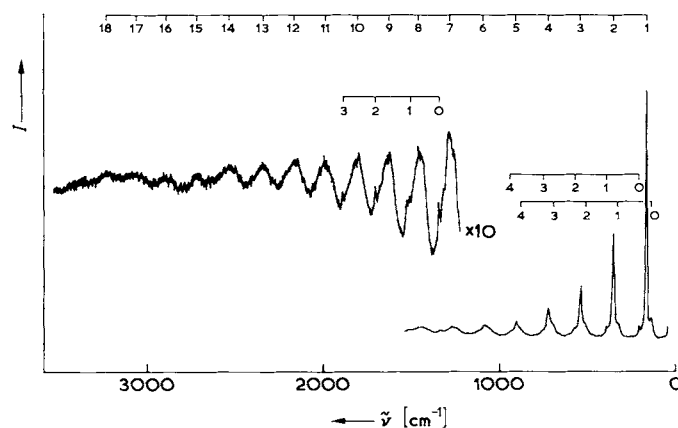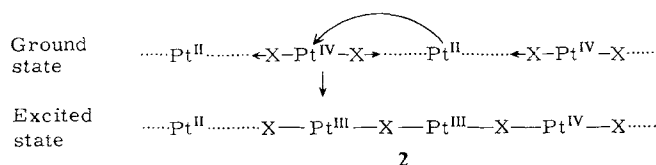

Fig. 23. Resonance Raman spectrum of $[Pt(tn)_2][Pt(tn)_2Br_2][ClO_4]_4$ in a KBr disk at ca. 80 K, obtained with 488.0 nm excitation (after Ref. [180]), tn = 1,3-diaminopropane.

indicate that the $Pt^{IV}-X$ bond lengths increase substantially (probably by at least 0.1 Å)[180] on excitation of the complex from the ground to the intervalence state. This structural change is precisely that expected (on conductance grounds) on excitation to the Pt^{III}/Pt^{III} intervalence state since, in its relaxed geometry in this state (as in 2), the axial halogen atoms would be expected to be midway between the Pt^{III} ions.

The assignment of the progression-forming mode to the symmetric chain-stretching vibration has been confirmed

Ground state $\quad \cdots\cdots Pt^{II}\cdots\cdots\leftarrow X-Pt^{IV}-X\rightarrow\cdots\cdots\cdots Pt^{II}\cdots\cdots\cdots\leftarrow X-Pt^{IV}-X\cdots\cdots$

Excited state $\quad \cdots\cdots Pt^{II}\cdots\cdots\cdots X - Pt^{III} - X - Pt^{III} - X - Pt^{IV} - X\cdots\cdots$

2

by single crystal orientation measurements, an example of which is shown in Figure 24.
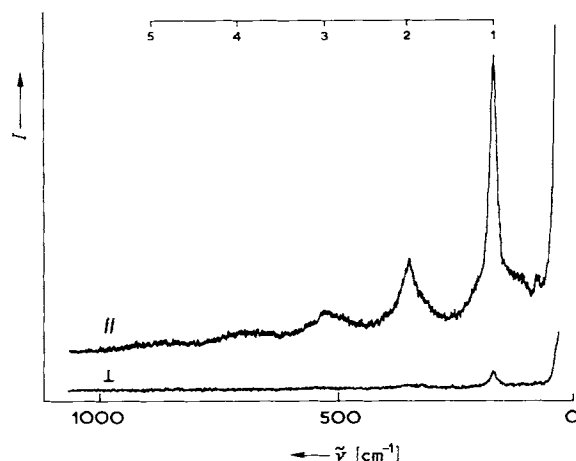
Fig. 24. Resonance Raman spectra of a single crystal of [Pt(tn)₂][Pt(tn)₂Br₂][ClO₄]₄ at ca. 298 K with the incident radiation polarized along the crystal Z axis and the scattered radiation ($\lambda_0 = 568.2$ nm) measured for polarization parallel and perpendicular to the Z axis (after Ref. [180]).

Related studies have been carried out on analogous mixed-valence Pd^{II}/Pd^{IV} chain complexes, and also on certain mixed-metal, mixed-valence complexes (e.g. Ni^{II}/Pt^{IV} and Pd^{II}/Pt^{IV} chain complexes), with similar results.[181-183] In all cases, harmonic wave numbers and anharmonicity constants have been calculated from the observed band wave numbers, and tabulated.[3] It has recently been discovered that, for certain linear-chain mixed-valence platinum complexes, the wave number, v_1, of the symmetric chain-stretching mode increases as the excitation wave number (v_0) increases.[184] For any set of complexes the wave-number change

$$v_1 (v_0 = \text{high wave number}) - v_1 (v_0 = \text{low wave number})$$

increases in the order $Cl < Br < I$ and is largest for those complexes in which the $Pt^{II} \cdots Pt^{IV}$ separation is least and for which the bond length ratio $r(Pt^{IV}-X)/r(Pt^{II}-X)$ is nearest to unity. This behavior, which is not observed for any of the equatorial modes, is believed to be due to solid state effects rather than an intrinsically mixed-valence property.

One other type of mixed-valence complex that is worthy of note is the so-called Creutz-Taube ion, [(NH₃)₅Ru(pyrazine)Ru(NH₃)₅]⁵⁺, in which the ruthenium oxidation states are formally +2 and +3 or both +2.5. Various spectroscopic techniques have led to conflicting conclusions concerning the electronic structure of this ion, especially on the extent of valence-delocalization.[185] RR spectra display several broad bands assigned to totally symmetric modes

which are probably associated with the pyrazine ring. However, the spectroscopic evidence obtained to date has not unequivocally established whether the odd electron is delocalized or trapped on one Ru atom, and further investigations are in progress. Another mixed-valence Ru^{II},Ru^{III} complex that has been investigated recently is [(NH₃)₃Ru(μ₃-X₃)Ru(NH₃)₃]²⁺ (X = Cl, Br, or I). Whereas the A'_1 ground state of this complex is localized (non-equivalent Ru centers), RR spectroscopy has indicated that, in the A''_2 excited state (14000-17000 cm⁻¹), the odd electron is delocalized.[186]

5.4. Metalloporphyrins

The study of metalloporphyrins and heme proteins by RR spectroscopy has developed into a major field of research since the pioneering work, over a decade ago, of *Spiro*.[25] Several comprehensive reviews of this subject have been written[5, 11, 26, 27] and it is our intention here to present only the essential features of metalloporphyrin RR spectra.

3
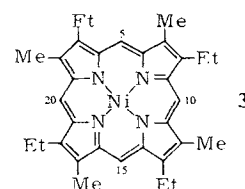
Absorption spectra of metalloporphyrins consist of an intense near UV band ($\varepsilon \approx 10^5$ M⁻¹ cm⁻¹), called the Soret band, and a weaker ($\varepsilon \approx 10^4$ M⁻¹ cm⁻¹) Q band in the visible region which displays a 0-0 and conglomerate 0-1 maxima. The positions of these bands vary considerably according to the central metal atom, its spin- and oxidation-state, and substituents on the metalloporphyrin ring (shown in Fig. 25) but typically the Soret band is at around 400-450 nm and the Q-band around 550-600 nm. Both bands are assigned to π-π^* ${}^1E_u \leftarrow {}^1A_{1g}$ transitions (in the idealized D_{4h} geometry) associated with the porphyrin ring. The electronic structures of metalloporphyrins have been investigated in some considerable detail by *Gouterman*,[187] and it has been shown that these two transitions arise from the promotion of electrons from filled, nearly degenerate, $1a_{1u}$ and $3a_{2u}$ orbitals to unfilled $4e_g$ orbitals. As a consequence of configuration interaction the transition to the higher energy Soret state is dipole-allowed while that to the Q state is nearly forbidden. Thus the latter transition acquires intensity by (Herzberg-Teller) vibronic coupling of the Soret and Q states, via a_{1g}, a_{2g}, b_{1g}, and b_{2g} vibrations, which give rise to the 0-1 conglomerate band.

RR spectra excited within the contour of the Q-band consist of the vibronically (B-term) active fundamentals of the porphyrin ring, which are distinguishable by their depolarization ratios: $\rho = 1/8$ (a_{1g}), $\rho = \infty$ (a_{2g}) and $\rho = 3/4$ (b_{1g} and b_{2g}). Deviations from these values bear witness to the lowering of the symmetry, especially to the loss of the fourfold axis, due to substituents on the porphyrin ring or to interaction with the environment within which the molecule is accommodated. Then, mixed symmetric/antisymmetric scattering may occur (see Section 2.5) giving

$3/4 < \rho < \infty$ for non-totally symmetric modes, and deviation from $\rho = 1/8$ might be observed for the totally symmetric modes. However, the latter are usually quite weak for Q-band excitation, and it may be impossible to obtain sufficiently accurate polarization data. Weak overtones of some of the non-totally symmetric fundamentals are sometimes observed, and have been ascribed to D-term scattering.

By contrast, RR spectra obtained by excitation within the contour of the Soret band are dominated by bands attributed to totally symmetric fundamentals. These owe their activity to an A-term scattering regime in which the displacement parameters are quite small. There have been far fewer studies of Soret-excited RR spectra, mainly because excitation in this region is not so widely available in most laboratories; however, it is expected that this situation will change, and that a wealth of experimental data will soon build up. In particular, Soret excitation offers the opportunity of monitoring the lowering of the symmetry (from D_{4h}) by measuring deviations of ρ from 1/8.

There have been several measurements of excitation profiles (mostly confined to the Q-band region). These have been analyzed in terms of contemporary RR theory. Typically, EPs display two maxima within the Q-band (0-0 and 0-1) which are of unequal intensity. For B-term scattering it is predicted that the 0-0 and 0-1 resonances are of equal intensity. As pointed out in Section 2.4, deviations from equal scattering intensity arise from (a) non-adiabatic coupling between the Q and Soret states, and (b) JT distortion in the Q state. The a_{2g} modes (those for which $\rho = \infty$) are not JT-active and therefore show only the non-adiabatic effect which favors the 0-1 resonance. Polarized ($\rho = 1/8$) and depolarized ($\rho = 3/4$) bands tend to show stronger 0-0 scattering, believed to arise from additional A-term contributions. Enhanced scattering in the 0-1 region can also arise from A-term/B-term interference.[45] Examples of all of these effects can be seen in the Q-band EPs of nickel aetioporphyrin I (see 3) (Fig. 25),[188] which represent the most complete Q-band profiles obtained for a symmetric metalloporphyrin.

The most detailed excitation profiles in the Soret region have been obtained for ferrocytochrome c (1362 cm^{-1} band) and ferricytochrome c (1374 cm^{-1} band) by Champion and Albrecht.[189] The EP of the former is asymmetric and has higher intensity in the 0-1 region, whereas the latter shows a broad structureless peak slightly blue-shifted from the 0-0 position. These observations were accounted for by a theoretical model encompassing both homogeneous and inhomogeneous broadening and a multidimensional subspace of vibrational and librational modes in the excited state. The latter was calculated analytically by approximating the product of Franck-Condon factors with the density of states to a truncated Lorentzian distribution. However, Shelnutt[190] has convincingly demonstrated that the enhanced scattering in the 0-1 region can be accounted for by a single-mode calculation including interference between inter- and intramanifold coupling (i.e. A-term/B-term interference).

In this short section we have attempted to present the essential features of metalloporphyrin RR scattering. As already pointed out a vast literature on this subject exists,
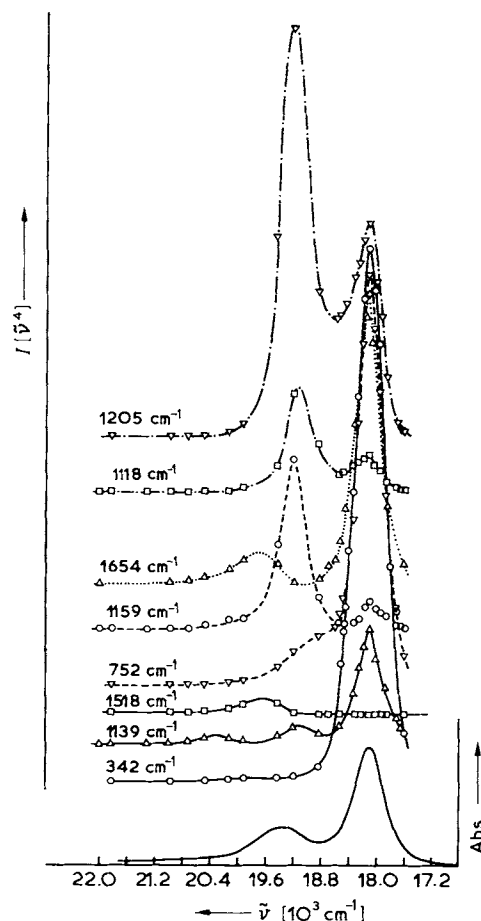

Fig. 25. Q-band resonance Raman excitation profiles of nickel(II) aetioporphyrin I in CDCl₃. Bands at 1118 and 1205 cm⁻¹ are inversely polarized, those at 752, 1159 and 1654 cm⁻¹ are depolarized, and those at 342, 1139 and 1518 cm⁻¹ are polarized. The uppermost excitation profile relates to the [5,10,15,20-D₄]-derivative (after Ref. [188]).

the major interest being concerned with biological aspects, such as electron transfer, respiratory function, catalysis, and metal transport or storage. Furthermore, the intricacies of the theoretical analysis of the spectra have become rather complicated due to the large number of phenomena involved. A recent paper by Shelnutt[19] is commended, in which is developed a simple model of vibronic states that brings out the essential features of metalloporphyrin RR spectra, excitation profiles, and polarization dispersion.

6. Conclusion and Future Outlook

The sensitivity of RR spectroscopy has transformed the technique of Raman spectroscopy from being one of greatly restricted use in inorganic and analytical chemistry to one of great value. Not only can species frequently be detected at very low concentrations by RR spectroscopy, but information is obtained specifically about the chromophoric center in the species. Since this part of a molecule is usually the one of greatest chemical interest—particularly in molecules of biochemical importance—increasing attention is being paid to RR studies of such species. Increasing attention is also being paid to the spectroscopy of molecules in excited electronic states, to the nature and spectroscopy of species generated at electrode surfaces, to ther-

mally sensitive species isolable only in matrices, and to the spectroscopy of transients in chemical reactions.

It is to be expected that, during the next few years, new developments of RR theory will considerably increase the amount of information obtainable from experimental data. In particular it is envisaged that more attention will be paid to the theoretical analysis of excitation profiles and to the polarization dispersion of Raman bands of molecules for which the absorption spectra are devoid of vibrational structure. In conjunction with the availability of a wider range of excitation lines, this will enable the RR technique for the determination of excited-state molecular geometries to be applied to a considerably larger number of inorganic molecules.

[1] R. J. H. Clark, B. Stewart, *Struct. Bonding (Berlin) 36* (1979) 1.
[2] D. F. Shriver, C. B. Cooper, *Adv. Infrared Raman Spectrosc. 6* (1980) 127.
[3] R. J. H. Clark, *Adv. Infrared Raman Spectrosc. 11* (1984) 95.
[4] R. J. H. Clark, *Chem. Soc. Rev. 13* (1984) 219.
[5] R. H. Felton, N.-T. Yu in D. Dolphin (ed.): *The Porphyrins, Vol. 3,* Academic Press, New York 1978, p. 347.
[6] P. Y. Yu, *Top. Curr. Phys. 14* (1979) 211.
[7] R. J. H. Clark, T. J. Dines, *Adv. Infrared Raman Spectrosc. 9* (1982) 282.
[8] G. H. Atkinson, *Adv. Infrared Raman Spectrosc. 9* (1982) 1.
[9] A. C. Albrecht, *J. Chem. Phys. 34* (1961) 1476.
[10] J. Tang, A. C. Albrecht, *Raman Spectrosc. 2* (1970) 33.
[11] P. M. Champion, A. C. Albrecht, *Annu. Rev. Phys. Chem. 33* (1982) 353.
[12] B. R. Stallard, P. M. Champion, P. R. Cullis, A. C. Albrecht, *J. Chem. Phys. 78* (1983) 712.
[13] P. P. Shorygin, *Pure Appl. Chem. 4* (1962) 87.
[14] L. L. Krushinskii, P. P. Shorygin, *Opt. Spectrosc. 11* (1961) 12, 80.
[15] J. Behringer, *Raman Spectrosc. 1* (1967) 168.
[16] J. Behringer, *Mol. Spectrosc. Chem. Soc., London [Specialist Periodical Reports] 2* (1974) 100; *3* (1976) 163.
[17] W. L. Peticolas, L. Nafie, P. Stein, B. Fanconi, *J. Chem. Phys. 52* (1970) 1576.
[18] B. B. Johnson, W. L. Peticolas, *Annu. Rev. Phys. Chem. 27* (1976) 465.
[19] J. A. Koningstein: *Introduction to the Theory of the Raman Effect,* D. Reidel, Dordrecht 1972.
[20] J. A. Koningstein, *Mol. Spectrosc. Chem. Soc., London [Specialist Periodical Reports] 4* (1977) 196.
[21] J. A. Koningstein, *Vib. Spectra Struct. 9* (1981) 115.
[22] D. L. Rousseau, J. M. Friedman, P. F. Williams, *Top. Curr. Phys. 11* (1979) 203.
[23] R. J. H. Clark, *Adv. Infrared Raman Spectrosc. 1* (1975) 143.
[24] R. J. H. Clark, B. Stewart, *J. Am. Chem. Soc. 103* (1981) 6593.
[25] T. G. Spiro, T. M. Loehr, *Adv. Infrared Raman Spectrosc. 1* (1975) 98.
[26] T. G. Spiro, P. Stein, *Annu. Rev. Phys. Chem. 28* (1977) 501.
[27] T. G. Spiro, *Phys. Bioinorg. Chem. Ser. 2* (1983) 89.
[28] W. Kiefer, *Adv. Infrared Raman Spectrosc. 3* (1977) 1.
[29] Y. Nishimura, A. Y. Hirakawa, M. Tsuboi, *Adv. Infrared Raman Spectrosc. 5* (1978) 217.
[30] A. Y. Hirakawa, M. Tsuboi, *Vib. Spectra Struct. 12* (1981) 145.
[31] O. S. Mortensen, S. Hassing, *Adv. Infrared Raman Spectrosc. 6* (1980) 1.
[32] W. Siebrand, M. Z. Zgierski, *Excited States 4* (1979) 1.
[33] L. D. Barron, E. N. Svendsen, *Adv. Infrared Raman Spectrosc. 8* (1981) 322.
[34] L. D. Barron, J. Vrbancich, *Adv. Infrared Raman Spectrosc. 12* (1985) 215.
[35] H.-K. Hong, *J. Chem. Phys. 67* (1977) 801, 813; *68* (1978) 1253.
[36] S.-Y. Lee, E. J. Heller, *J. Chem. Phys. 71* (1979) 4777.
[37] D. J. Tannor, E. J. Heller, *J. Chem. Phys. 77* (1982) 202.
[38] R. J. H. Clark, T. J. Dines, *Mol. Phys. 42* (1981) 193; *45* (1982) 1153.
[39] H. A. Kramers, W. Heisenberg, *Z. Phys. 31* (1925) 681.
[40] O. S. Mortensen, E. N. Svendsen, *J. Chem. Phys. 74* (1981) 3185.
[41] G. Herzberg, E. Teller, *Z. Phys. Chem. 21* (1933) 410.
[42] C. Manneback, *Physica 17* (1951) 1001.
[43] A. P. Penner, W. Siebrand, *Chem. Phys. Lett. 39* (1976) 11.
[44] W. Siebrand, M. Z. Zgierski, *J. Phys. Chem. 86* (1982) 4718.

[45] R. J. H. Clark, T. J. Dines, *Chem. Phys. Lett. 79* (1981) 321.
[46] L. D. Ziegler, B. S. Hudson, *J. Chem. Phys. 79* (1983) 1197.
[47] A. Y. Hirakawa, M. Tsuboi, *Science 188* (1975) 359.
[48] G. J. Small, E. S. Yeung, *Chem. Phys. 9* (1975) 379.
[49] D. A. Long: *Raman Spectroscopy,* McGraw-Hill, New York 1977.
[50] H. Hamaguchi, *J. Chem. Phys. 66* (1977) 5757; *69* (1978) 569.
[51] R. J. H. Clark, P. C. Turtle, *J. Chem. Soc. Faraday Trans. 2 72* (1976) 1885.
[52] R. J. H. Clark, T. J. Dines, *Chem. Phys. 70* (1982) 269.
[53] M. Pawlikowski, M. Z. Zgierski, *Chem. Phys. Lett. 48* (1977) 201; *J. Raman Spectrosc. 7* (1978) 106.
[54] M. Pézolet, L. A. Nafie, W. L. Peticolas, *J. Raman Spectrosc. 1* (1973) 455.
[55] J. Nestor, T. G. Spiro, *J. Raman Spectrosc. 1* (1973) 539.
[56] P. Stein, J. M. Brown, T. G. Spiro, *Chem. Phys. 25* (1977) 237.
[57] P. W. Jensen, *Chem. Phys. Lett. 77* (1981) 267.
[58] P. Stein, P. W. Jensen, T. G. Spiro, *Chem. Phys. Lett. 80* (1981) 451.
[59] R. D. Peacock, B. Stewart, *J. Raman Spectrosc. 15* (1984) 396.
[60] K. Manzel, V. Engelhardt, H. Abe, W. Schulze, F. W. Froben, *Chem. Phys. Lett. 77* (1981) 514.
[61] F. Ahmed, E. R. Nixon, *J. Chem. Phys. 74* (1981) 2156; *75* (1981) 110.
[62] R. Willbrandt, N.-H. Jensen, A. H. Sillesen, K. B. Hansen, *Chem. Phys. Lett. 106* (1984) 503.
[63] V. E. Bondybey, J. H. English, *Chem. Phys. Lett. 60* (1978) 69.
[64] J. C. Miller, L. Andrews, *J. Chem. Phys. 68* (1978) 1701.
[65] D. P. DiLella, W. Limm, R. H. Lipson, M. Moskovits, K. V. Taylor, *J. Chem. Phys. 77* (1982) 5263.
[66] M. Moskovits, D. P. DiLella, *J. Chem. Phys. 73* (1980) 4917.
[67] M. Moskovits, D. P. DiLella, W. Limm, *J. Chem. Phys. 80* (1984) 626.
[68] K. Manzel, W. Schulze, F. W. Froben, *Chem. Phys. Lett. 82* (1981) 557.
[69] D. D. Stranz, R. K. Khanna, *J. Chem. Phys. 74* (1981) 2116.
[70] H. Sontag, B. Eberle, R. Weber, *Chem. Phys. 80* (1983) 279.
[71] R. J. H. Clark, D. G. Cobbold, *Inorg. Chem. 17* (1978) 3169.
[72] R. J. H. Clark, T. J. Dines, M. Kurmoo, *Inorg. Chem. 22* (1983) 2766.
[73] R. A. Teichman, M. Epting, E. R. Nixon, *J. Chem. Phys. 68* (1978) 336.
[74] M. A. Epting, M. T. McKenzie, E. R. Nixon, *J. Chem. Phys. 73* (1980) 134.
[75] C. Cossé, M. Fonassier, T. Mejean, M. Tranquille, D. P. DiLella, M. Moskovits, *J. Chem. Phys. 73* (1980) 6076.
[76] L. Stein, J. R. Norris, A. J. Downs, A. R. Minihan, *J. Chem. Soc. Chem. Commun. 1978,* 502.
[77] H. Chang, D.-M. Hwang, *J. Chem. Phys. 67* (1977) 3624.
[78] J. A. Coxon, N. Gramari, M. Jacon, *J. Raman Spectrosc. 8* (1979) 63.
[79] O. Atabek, R. Lefebvre, M. Jacon, *J. Chem. Phys. 72* (1980) 2683.
[80] H. Chang, D.-M. Hwang, *J. Chem. Phys. 67* (1977) 4777.
[81] H. Chang, D.-M. Hwang, *J. Raman Spectrosc. 7* (1978) 254.
[82] F. Ghandow, M. Jacon, E. N. Svendsen, J. Oddershede, *J. Chem. Phys. 79* (1983) 2150.
[83] H. H. Eysel, H. J. Bernstein, *J. Raman Spectrosc. 6* (1977) 140.
[84] M. T. Bourgeois, M. Jacon, D. Van Labeke, H. H. Eysel, *J. Raman Spectrosc. 6* (1977) 146.
[85] D. P. DiLella, K. V. Taylor, M. Moskovits, *J. Phys. Chem. 87* (1983) 524.
[86] L. Andrews, E. S. Prochaska, A. Loewenschuss, *Inorg. Chem. 19* (1980) 463.
[87] M. Moskovits, D. P. DiLella, *J. Chem. Phys. 72* (1980) 2267.
[88] F. Bolduan, H. J. Jodl, *J. Mol. Spectrosc. 91* (1982) 404.
[89] J. B. Bates, *J. Chem. Phys. 69* (1978) 1934.
[90] G. M. Gualberto, M. A. Tenan, H. Vegers, L. C. M. Miranda, J. Peizl, *Phys. Rev. B17* (1978) 919.
[91] L. C. Campelo, F. E. A. Melo, J. M. Filho, R. S. Katiyar, H. Vargas, *J. Raman Spectrosc. 10* (1981) 33.
[92] J. Bojes, T. Chivers, W. G. Laidlaw, M. Trsic, *J. Am. Chem. Soc. 104* (1982) 4837.
[93] H. Sontag, R. Weber, *Chem. Phys. 70* (1982) 23.
[94] H. Schnöckel, H.-J. Goecke, R. Elsper, *Z. Anorg. Allg. Chem. 494* (1982) 78.
[95] H. Schnöckel, *Z. Anorg. Allg. Chem. 510* (1984) 72.
[96] L. D. Ziegler, B. Hudson, *J. Phys. Chem. 88* (1984) 1110.
[97] R. J. H. Clark, T. J. Dines, L. T. H. Ferris, *J. Chem. Soc. Dalton Trans. 1982,* 2237.
[98] R. J. H. Clark, T. J. Dines, *Inorg. Chem. 21* (1982) 3585.
[99] E. Campani, F. Ferri, G. Gorini, E. Polacco, G. Masetti, *Chem. Phys. Lett. 107* (1984) 91.
[100] L. D. Barron, C. Meehan, *Chem. Phys. Lett. 66* (1979) 444.
[101] R. J. H. Clark, T. J. Dines, *Inorg. Chem. 19* (1980) 1681.
[102] R. J. H. Clark, D. G. Cobbold, B. Stewart, *Chem. Phys. Lett. 69* (1980) 488.
[103] R. J. H. Clark, T. J. Dines, *J. Chem. Soc. Faraday Trans. 2 78* (1982) 723.
[104] A. H. Jubert, E. L. Varetti, *J. Mol. Struct. 79* (1982) 285.
[105] A. H. Jubert, E. L. Varetti, *J. Raman Spectrosc. 13* (1982) 83.

Angew. Chem. Int. Ed. Engl. 25 (1986) 131–158

157

[106] A. H. Jubert, S. G. Manca, E. J. Baran, E. L. Varetti, *Z. Anorg. Allg. Chem. 492* (1982) 197.

[107] H. Homborg, *Z. Anorg. Allg. Chem. 498* (1983) 25.

[108] A. H. Jubert, E. L. Varetti, E. J. Baran, *J. Raman Spectrosc. 15* (1984) 139.

[109] T. P. Martin, S. Onari, *Phys. Rev. B 15* (1977) 1093.

[110] R. J. H. Clark, T. J. Dines, J. M. Doherty, *Inorg. Chem. 24* (1985) 2088.

[111] E. Königer-Ahlborn, A. Müller, *Spectrochim. Acta A 33* (1977) 273.

[112] R. J. H. Clark, T. J. Dines, M. L. Wolf, *J. Chem. Soc. Faraday Trans. 2 78* (1982) 679.

[113] M. L. A. Temperini, O. Sala, H. J. Bernstein, *Chem. Phys. Lett. 59* (1978) 10.

[114] R. J. H. Clark, T. J. Dines, *Chem. Phys. Lett. 64* (1979) 499.

[115] R. J. H. Clark, T. J. Dines, G. P. Proud, *J. Chem. Soc. Dalton Trans. 1983*, 2019.

[116] L. W. Johnson, S. P. McGlynn, *Chem. Phys. Lett. 7* (1970) 618.

[117] C. J. Ballhausen, I. B. Trabjerg, *Mol. Phys. 24* (1972) 689.

[118] R. J. H. Clark, P. C. Turtle, *J. Chem. Soc. Dalton Trans. 1977*, 2142.

[119] L. Tosi, A. Garnier, *J. Chem. Soc. Dalton Trans. 1978*, 53.

[120] O. Siiman, *Inorg. Chem. 19* (1980) 2889.

[121] R. Czernuszewicz, E. Maslowsky, K. Nakamoto, *Inorg. Chim. Acta 40* (1980) 199.

[122] R. Czernuszewicz, G. Y. Lim, D. T. Haworth, K. Nakamoto, *Inorg. Chim. Acta 44* (1980) L 167.

[123] R. S. Czernuszewicz, K. Nakamoto, D. P. Strommen, *J. Am. Chem. Soc. 104* (1982) 1515.

[124] W. Preetz, G. Peters, *Z. Naturforsch. B 35* (1980) 1355.

[125] G. Peters, W. Preetz, *Z. Naturforsch. B 36* (1981) 138.

[126] R. J. H. Clark, P. C. Turtle, *J. Chem. Soc. Faraday Trans. 2 74* (1978) 2063.

[127] H. Homborg, *Z. Anorg. Allg. Chem. 493* (1982) 104, 121.

[128] L. D. Barron, J. Vrbancich, R. S. Watts, *Chem. Phys. Lett. 89* (1982) 71.

[129] R. J. H. Clark, P. C. Turtle, *Chem. Phys. Lett. 51* (1977) 265.

[130] H. Hamaguchi, M. Tasumi, *J. Chem. Phys. 78* (1983) 131.

[131] L. D. Barron, C. Meehan, J. Vrbancich, *Mol. Phys. 41* (1980) 945.

[132] L. D. Barron, J. Vrbancich, *J. Raman Spectrosc. 14* (1983) 118.

[133] H. Homborg, *Z. Anorg. Allg. Chem. 460* (1980) 17, 27.

[134] K.-I. Ikeda, S. Maeda, *Inorg. Chem. 17* (1978) 2698.

[135] W. Preetz, M. Bruns, *Z. Naturforsch. B 38* (1983) 680.

[136] R. J. H. Clark, T. J. Dines, *Mol. Phys. 52* (1984) 859.

[137] R. J. H. Clark, M. J. Stead, *Chem. Phys. 91* (1984) 113.

[138] C. Sourisseau, Y. Mathey, *Chem. Phys. Lett. 74* (1980) 128; *Chem. Phys. 63* (1981) 143.

[139] S. P. Gwet, Y. Mathey, C. Sourisseau, *Phys. Status Solidi B 123* (1984) 503.

[140] R. J. H. Clark, P. C. Turtle, D. P. Strommen, B. Streusand, J. Kincaid, K. Nakamoto, *Inorg. Chem. 16* (1977) 84.

[141] B. Streusand, A. T. Kowal, D. P. Strommen, K. Nakamoto, *J. Inorg. Nucl. Chem. 39* (1977) 1767.

[142] P. J. Miller, R. S.-L. Chao, *J. Raman Spectrosc. 8* (1979) 17.

[143] R. S. Czernuszewicz, K. Nakamoto, D. P. Strommen, *Inorg. Chem. 19* (1980) 793.

[144] P. W. Jensen, *Chem. Phys. Lett. 77* (1981) 267.

[145] L. Griffiths, B. P. Straughan, D. J. Gardiner, *J. Chem. Soc. Dalton Trans. 1983*, 305.

[146] R. F. Dallinger, W. H. Woodruff, *J. Am. Chem. Soc. 101* (1979) 4391.

[147] M. Forster, R. E. Hester, *Chem. Phys. Lett. 81* (1981) 42.

[148] P. G. Bradley, N. Kress, B. A. Homberger, R. F. Dallinger, W. H. Woodruff, *J. Am. Chem. Soc. 103* (1981) 7441.

[149] M. Basu, H. D. Gafney, T. C. Strekas, *Inorg. Chem. 21* (1982) 2231.

[150] R. W. Balk, D. J. Stufkens, R. J. Crutchley, A. B. P. Lever, *Inorg. Chim. Acta 64* (1982) L 49.

[151] W. K. Smothers, M. S. Wrighton, *J. Am. Chem. Soc. 105* (1983) 1067.

[152] S. McClanahan, T. Hayes, J. Kincaid, *J. Am. Chem. Soc. 105* (1983) 4486.

[153] J. Ferguson, F. Herren, *Chem. Phys. Lett. 89* (1982) 371; J. Ferguson, F. Herren, G. M. McLaughlin, *ibid. 89* (1982) 376; J. Ferguson, F. Herren, *Chem. Phys. 76* (1983) 45.

[154] D. J. Stufkens, *J. Mol. Struct. 79* (1982) 67, and references cited therein.

[155] R. W. Balk, D. J. Stufkens, A. Oskam, *J. Chem. Soc. Dalton Trans. 1982*, 275.

[156] M. W. Kokkes, D. J. Stufkens, A. Oskam, *J. Chem. Soc. Dalton Trans. 1983*, 439.

[157] D. J. Stufkens, M. W. Kokkes, A. Oskam, *J. Mol. Struct. 114* (1984) 61.

[158] Y.-Y. Yang, J. I. Zink, *J. Am. Chem. Soc. 106* (1984) 1500.

[159] T. Ziegler, A. Rauk, E. J. Baerends, *Chem. Phys. 16* (1976) 209.

[160] F. A. Cotton, R. A. Walton: Metal Atoms, Wiley-Interscience, New York 1982.

[161] R. J. H. Clark, M. L. Franks, *J. Am. Chem. Soc. 97* (1975) 2691.

[162] R. J. H. Clark, M. L. Franks, *J. Am. Chem. Soc. 98* (1976) 2763.

[163] R. J. H. Clark, N. R. D'Urso, *J. Am. Chem. Soc. 100* (1978) 3088.

[164] W. Preetz, L. Rudzik, *Angew. Chem. 91* (1979) 159; *Angew. Chem. Int. Ed. Engl. 18* (1979) 150.

[165] W. Preetz, G. Peters, L. Rudzik, *Z. Naturforsch. B 34* (1979) 1240.

[166] H. D. Glicksman, R. A. Walton, *Inorg. Chem. 17* (1978) 3197.

[167] R. J. H. Clark, M. J. Stead in M. H. Chisholm (ed.): *Inorganic Chemistry: Toward the 21st Century*, ACS Symp. Ser. No. 211, 1983, p. 235.

[168] R. J. H. Clark, M. J. Stead, *Inorg. Chem. 22* (1983) 1214.

[169] R. J. H. Clark, L. T. H. Ferris, *Inorg. Chem. 20* (1981) 2759.

[170] R. J. H. Clark, A. J. Hempleman, H. M. Dawes, M. B. Hursthouse, C. D. Flint, *J. Chem. Soc. Dalton Trans. 1985*, 1775.

[171] R. J. H. Clark, A. J. Hempleman, C. D. Flint, *J. Am. Chem. Soc.*, in press.

[172] R. J. H. Clark, M. L. Franks, P. C. Turtle, *J. Am. Chem. Soc. 99* (1977) 2473.

[173] J. R. Campbell, R. J. H. Clark, *Mol. Phys. 36* (1978) 1133; *J. Chem. Soc. Faraday Trans. 2 76* (1980) 1103.

[174] J. R. Campbell, R. J. H. Clark, *J. Chem. Soc. Dalton Trans. 1981*, 1239.

[175] J. R. Campbell, R. J. H. Clark, M. J. Stead, *J. Chem. Soc. Dalton Trans. 1983*, 2005.

[176] R. E. Hester, E. M. Nour, *J. Raman Spectrosc. 11* (1981) 43, 49, 59, 64.

[177] A. Müller, A.-M. Dommröse, W. Jaegermann, E. Krickemeyer, S. Sarkar, *Angew. Chem. 93* (1981) 1119; *Angew. Chem. Int. Ed. Engl. 20* (1981) 1061.

[178] A. Müller, R. R. Filgueira, W. Jaegermann, S. Che, *Naturwissenschaften 68* (1981) 93.

[179] R. J. H. Clark, T. J. Dines, G. P. Proud, *J. Chem. Soc. Dalton Trans. 1983*, 2299.

[180] R. J. H. Clark, M. Kurmoo, *Inorg. Chem. 19* (1980) 3522.

[181] R. J. H. Clark, V. B. Croud, M. Kurmoo, *Inorg. Chem. 23* (1984) 2499.

[182] S. D. Allen, R. J. H. Clark, V. B. Croud, M. Kurmoo, *Phil. Trans. Roy. Soc. A 314* (1985) 131.

[183] R. J. H. Clark, V. B. Croud, *Inorg. Chem. 24* (1985) 588.

[184] R. J. H. Clark, M. Kurmoo, *J. Chem. Soc. Faraday Trans. 2 79* (1983) 519.

[185] U. Fürholz, H.-B. Bürgi, F. E. Wagner, A. Stebler, J. H. Ammeter, E. Krausz, R. J. H. Clark, M. J. Stead, A. Ludi, *J. Am. Chem. Soc. 106* (1984) 121.

[186] R. S. Armstrong, J. K. Beattie, P. del Favero, V. M. Ellis, N. S. Hush, *Inorg. Chim. Acta 89* (1984) L 33.

[187] M. Gouterman in D. Dolphin (ed.): *The Porphyrins, Vol. 3*, Academic Press, New York 1978, p. 1.

[188] J. A. Shelnutt, L. D. Cheung, R. C. C. Chang, N.-T. Yu, R. H. Felton, *J. Chem. Phys. 66* (1977) 3387.

[189] P. M. Champion, A. C. Albrecht, *J. Chem. Phys. 71* (1979) 1110; *72* (1980) 6498.

[190] J. A. Shelnutt, *J. Chem. Phys. 72* (1980) 3948.

[191] J. A. Shelnutt, *J. Chem. Phys. 74* (1981) 6644.

158

Angew. Chem. Int. Ed. Engl. 25 (1986) 131-158